Hindawi
Geofluids
Volume 2021, Article ID 5762201, 29 pages
https://doi.org/10.1155/2021/5762201

Research Article

Experimental Study on Creep Behavior and Crack Evolution of Stratified Structural Sandstone under Segmental Constant Load

Yiran Yang[1], **Yanzhong Li**[2], **Jiaojiao Pan**[1], **Tao Luo**[1] and **Zidong Lu**[3]

[1]*Shaanxi Key Laboratory of Safety and Durability of Concrete Structures, School of Civil Engineering, Xijing University, Xi'an, Shaanxi Province 710123, China*
[2]*State Key Laboratory of Mining Response and Disaster Prevention and Control in Deep Coal Mines, College of Mechanical Engineering, Anhui University of Science and Technology, Huainan, Anhui Province 232001, China*
[3]*Yunnan Branch of Jianyin Engineering Consulting Co., Ltd., Kunming, Yunnan Province 650011, China*

Correspondence should be addressed to Yanzhong Li; liyanzhong415@163.com

Received 21 April 2021; Accepted 20 July 2021; Published 12 August 2021

Academic Editor: Yonghui Wu

The hazards induced by stratified rock mass creep are still one of the major problems that threaten the safety of underground engineering. This paper takes safe construction of underground roadway in Urumqi mining area as the research background. In this study, we mainly adopted rock mechanics experiments to accomplish the research on creep behavior and crack evolution of stratified structural sandstone. Creep deformation characteristics of stratified structural sandstone under different load were revealed; also, we analyzed the reason why a part of rock samples failed but others were not under the same load. Creep behavior and crack evolution of rock samples without stratified structure have significant randomness. The crack evolution and failure characteristics of stratified structural rock samples were mainly manifested as failure along and cutting through structural plane and their combined forms. Creep strain, creep duration, and creep rate of rock samples with stratified structure had a nonlinear relationship with applied load, such as exponential function or logarithmic function. Understanding the evolutionary relationship between the above parameters and load provides a basis for obtaining the creep behavior of stratified rock mass under different load conditions.

1. Introduction

Creep of rock is common in the underground engineering, which leads to time-sensitive characteristics of crack evolution in rock deformation [1–3]. In terms of deep rock engineering construction, the service time of large underground tunnel increases obviously, and the general expected life is from several decades to more than a hundred years. Therefore, it is necessary to consider time-dependent properties of rock mass in the design, construction, and routine maintenance [4–6]. Particularly when in situ stress is less than short-term strength of rock mass and original layered structure exists in the rock mass, it is easy to generate creep and crack propagation [7, 8]. Therefore, it is important for disaster control to study the development of creep deformation and crack evolution of deep rock mass.

An experimental study is an effective method to obtain the creep behavior and typical parameters of rock mass, which is widely favored by researchers due to its advantages of rapidity and intuitive. Especially in recent years, with improvement and upgrading of experimental equipment, application scope of experimental research has been promoted and expanded to a large extent. Researchers optimized and improved experimental equipment according to their requirements, which accelerated the process of rock mass creep research. Liu et al. [9] studied creep behavior and characteristic of saturated rock under high stress in uniaxial single-stage load and graded incremental cyclic load mode, providing a basis for deformation control and disaster relief of deep saturated rock mass. Dubey and Gairola [10] used experimental means to study the influence of internal anisotropy of rock salt on its creep behavior and control effect.

They believed that structural anisotropy had a strong control effect on the development of instantaneous strain, transient strain, steady strain, and accelerated strain, and the influence of structural anisotropy on rock salt deformation had a negative correlation with the stress level. Zivaljevic and Tomanovic [11] adopted a uniaxial creep experimental method to analyze the creep characteristics and behavior of marl, focusing on the influence of compressive stress preconsolidation level and load time on the creep parameters of marl. Pellet and Fabre [12] carried out static, quasistatic, and cyclic creep experiments on sedimentary rock, and the results showed that the content of clay particles had a significant impact on the creep behavior, and the creep of particles had an adverse effect on the creep behavior. Rahimi and Hosseini [13] carried out triaxial creep experiments on thick-walled hollow columnar rock salt samples to study the effects of confining pressure, eccentricity stress, and strain rate on the creep behavior of rock salt. The results showed that the strain rate increased with the increase of eccentricity stress and confining pressure, and the lateral pressure was more important than the eccentricity stress in the change of tangential strain rate. Grgic and Amitrano [14] studied the influence of water saturation on rock creep by multistep uniaxial creep experiments of polycrystalline porous rocks under partially saturated conditions and explained the important role of microcrack in the creep process by analyzing strain and acoustic emission monitoring data.

Nadimi et al. [15] carried out triaxial creep experiments on the rock and obtained the creep characteristics of the rock mass around the cave. They estimated the parameters of a dynamic constitutive creep model by using the creep experiment and field measured data, which made it possible to simulate the primary and secondary creep zones of rock mass. The calculated results are in good agreement with the measured data, providing a theoretical basis for the support design of underground engineering. Herrmann et al. [16] explored the creep behavior and mechanism of different types of shale through the creep experimental method under high confining pressure and variable temperature control. The results showed that under high temperature, axial differential pressure stress, and low confining pressure, the creep strain of shale increased. The initial creep strain was related to the mechanical properties determined by short-term constant strain rate experiments, such as static Young's modulus and triaxial compressive strength. Rybacki et al. [17] simulated the occurrence environment of shale under high stress, high temperature, and low constraint conditions caused by the increase of field depth. The results showed that the sample exhibited semibrittle creep with high deformation rate, and the strain was mainly regulated by the deformation of weak organic matter, layered silicate, and the reduction of pore space. Bhat and Bhandary [18] improved the torsional ring shearing instrument, measured the displacement variation with time under constant creep stress, studied the creep behavior of typical clay in the residual state, and proposed the creep failure prediction curve in the residual state, which provided a basis for the prediction of creep landslide failure time and displacement. Bagheri et al. [19] conducted triaxial creep experiments on clay samples under different shear stress levels and strain rates, measured their volumetric strain rates, and determined the relationship between the nonlinear variation of stress and initial volumetric strain rates.

Fabre and Pellet [20] carried out creep experiments on argillaceous rocks under a variety of stress environments and found that the overall mechanical properties of argillaceous rocks deteriorated rapidly when the cracks propagated unsteadily, and the creep of clay particles caused viscoplastic strain. Brantut et al. [21] proposed a micromechanical model that could describe the brittle creep of saturated rock under triaxial stress with time and studied the micromechanics of brittle creep. Davis et al. [22] carried out triaxial compression experiments on dolomites with different particle sizes under variable temperature conditions and revealed the differences of creep mechanism between coarse-grained dolomites and fine-grained dolomites with different grain sizes. Smit et al. [23] studied the structure and microstructure of garnet polycrystals in eclogites and analyzed the creep mechanism of garnet in eclogites by using optical microscopy, element mapping, and electron backscatter diffraction. Rybacki and Dresen [24] carried out creep experiments on plagioclase samples under dry and wet conditions and determined two different creep mechanisms of dry and wet plagioclase. Heap et al. [25] studied the creep mechanism of pore water in sandstone by using microstructure analysis, acoustic emission source location, and macroscopic creep law. Brückl and Parotidis [26] analyzed the deep creep mechanism of slope rock mass with simulation study and pointed out that the main factor controlling the deep creep mechanism was the expansion of subcritical cracks. Bresser [27] obtained the pressure sensitivity and strain rate sensitivity of flow stress through experiments and revealed the creep mechanism of calcite dislocation at high temperature based on the experimental data of microphysical model. Gratier et al. [28] carried out indentation experiments on quartz crystals, which provided characteristic time scales for the transient creep and sealing processes of quartz-rich rocks after earthquakes.

Researches have carried out experiments on rock without primary structures and obtained instructive results [29–31]. However, stratified structural rock mass widely exists in deep engineering, and it is characterized by structural anisotropy. Related studies have found that structural anisotropy has a controlling effect on the creep behavior and crack evolution of rock mass. Therefore, the study on creep behavior and law of stratified structural rock is of guiding significance to discover the failure mechanism of such rock mass. Also, it is an important supplement to the study of rock mechanics. The rock samples used in this study were taken from the surrounding rock of underground roadway in Urumqi mining area. Through systematic creep experiments under different loads, the control effect of structural anisotropy on creep of stratified structural rock samples was studied. And the degree of difference in deformation rate caused by structural anisotropy in rock samples was analyzed to obtain the creep behavior and crack evolution of stratified structural rock mass.

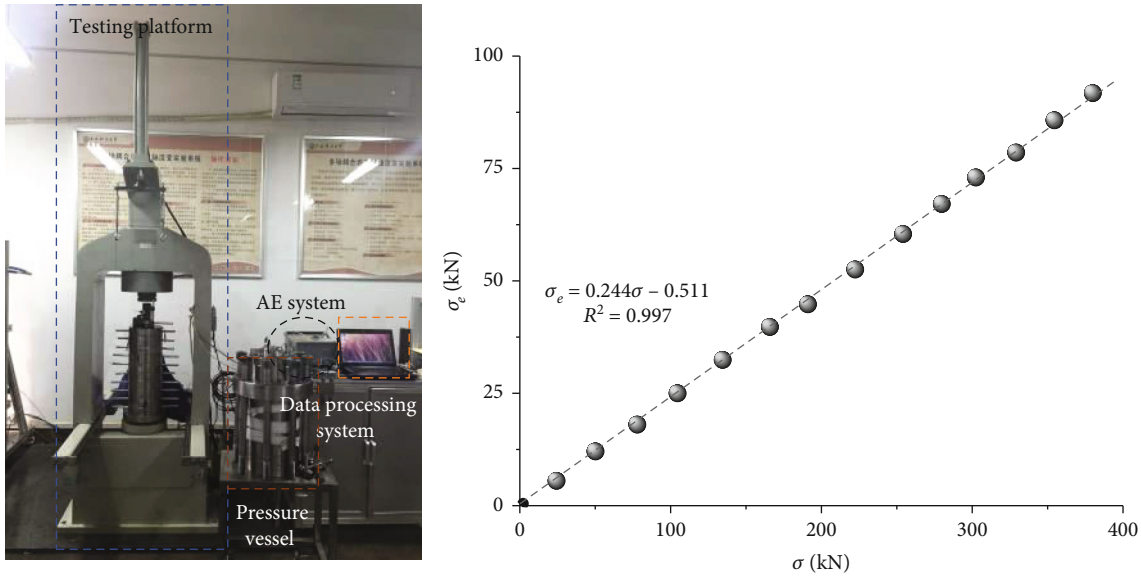

Figure 1: THMC rheological test system for rock.

2. Materials and Methods

2.1. Uniaxial Creep Experiment Procedure and Preliminary Preparation. The uniaxial creep experiment proposed in this study adopted the measurement method recommended by ISRM (2014) and the ASTM (2008). During the experiment, the relative humidity was controlled by saturated sodium nitrate solution, and the relative humidity should be maintained at 40% at 20°C. The variation range of relative humidity and laboratory temperature was generally maintained at ±5.0% and ±1.0°C, respectively.

The THMC rheological test system was mainly used in the experiment. And, its calibration curve showed that the relationship between the effective stress σ_e and the applied stress σ is $\sigma_e = 0.244\sigma$-0.511 (Figure 1). Other equipment included strain gauges, SWAES digital multichannel acoustic emission devices, and digital cameras. Axial strain and radial strain were measured by strain gauge and DD1 cantilever strain sensor produced by HBM Company. We used the RMT-150C rock and concrete mechanics test system to conduct the experiment. The size of samples was the same as the ones used in the creep experiments. The number of rock samples was 12.

The samples were divided into four groups according to the differences of their internal structure (Table 1). The compressive loads equivalent to 50%, 60%, 70%, and 80% of uniaxial compressive strength (σ_c) are applied to samples without a stratified structure to simulate the in situ stress state generated by overburden geological body and tectonic stress in the natural environment. Compressive loads equivalent to 30%, 40%, 50%, 60%, 70%, 75%, 80%, and 85% of uniaxial compressive strength were applied to the samples, respectively. The loads were carried out by stress control method, and the load rate was controlled as 0.01 kN/s. In the initial stage of creep experiment, the experimental parameters were read and recorded at intervals of 1.0 min, 5.0 min, and 10.0 min, and then, the interval was extended to 0.5-1.0 h in the middle stage of experiment. Finally, at the end of the experiment, when the rock sample was close to failure, the reading interval was changed to be 10.0 min, 5.0 min, and 1.0 min.

Table 1: Statistics of rock sample parameters.

Serial number	Feature	Average angle	Amount
USN	None	None	4
USH	Horizontal	2.5°	8
USO	Oblique	45.0°	8
USV	Vertical	87.0°	8

3. Results and Discussion

3.1. Creep Characteristics of the USN Rock Samples. Creep experiments of rock samples without stratified structures were carried out at stress levels close to the average value of C_i threshold and C_d threshold. In these experiments, the target constant load was applied and maintained by controlling the axial load, and the strain variation and increment were monitored and recorded at the same time.

Figure 2(a) shows the state of USN-1 rock sample under load of 50% σ_c. The sample had the first and second creep stages, in which the sample exhibited such changes as end slag shedding, axial shrinkage, and radial expansion. However, during the experiment lasting for 240.0 h, the creep process did not enter the third creep stage but gradually had a stable state. Statistical results of AE monitoring data showed that there was basically no AE signal between 15.0 h and 240.0 h, indicating that the evolution of crack inside the sample was gradually weakening. The failure characteristics of USN-2 rock sample were obviously random,

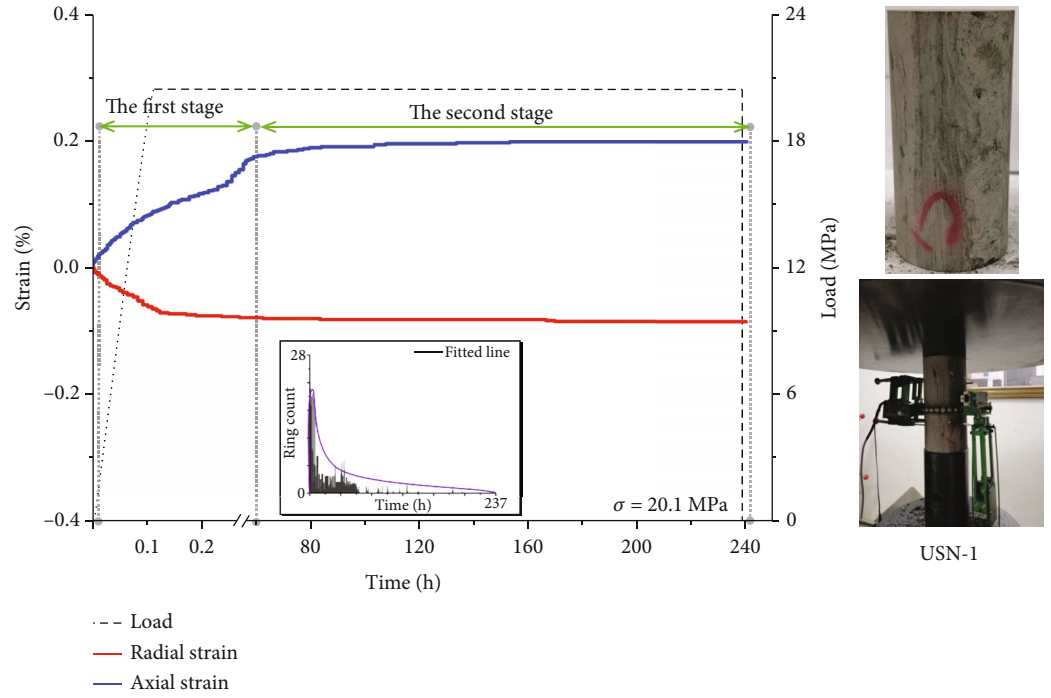

(a)

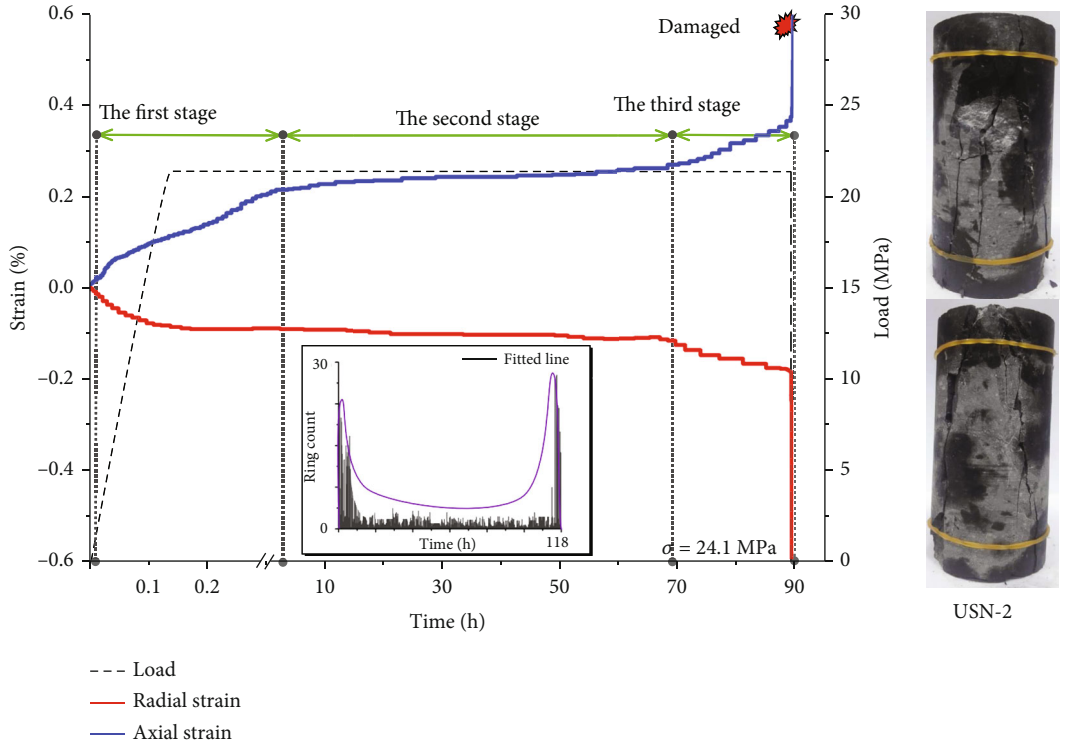

(b)

Figure 2: Continued.

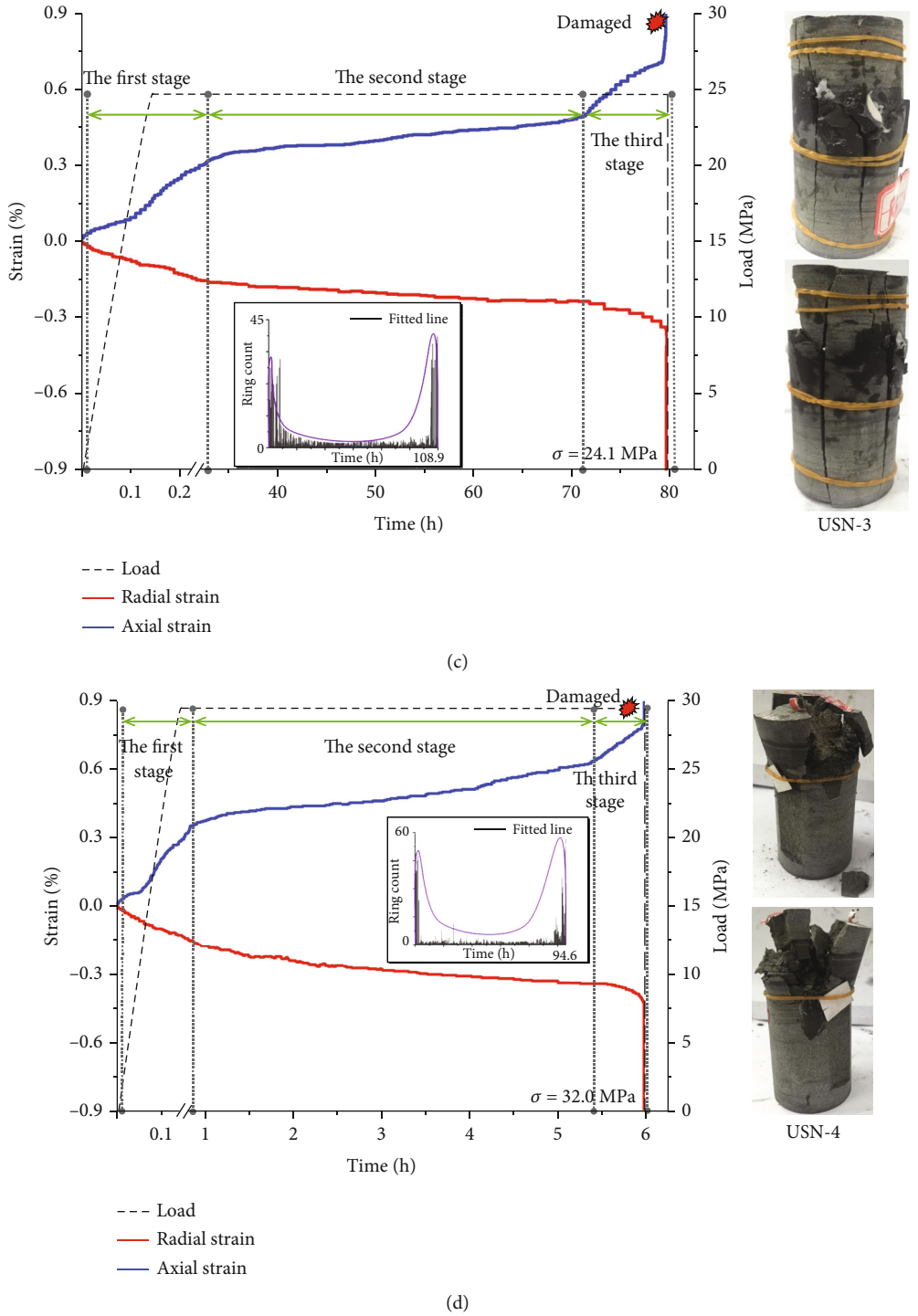

Figure 2: Creep test curve of USN rock samples.

and the crack evolution was irregular (Figure 2(b)). Failure of this sample was dominated by oblique crack, and the angle between the oblique crack and the horizontal plane was different in size, which was not statistical. At the intersection of anisotropic cracks, the shallow part of the sample collapsed in layers or small blocks, which accelerated the overall failure of the sample. Due to the energy absorption effect, there was no large crack throughout the whole sample, so the damaged sample still had a certain residual strength.

Due to the sudden instability of the USN-3 rock sample, the transition characteristics of creep from the second stage to the third stage were not clear (Figure 2(c)). To some extent, this might lead to the overlap of creep stages, which made it hard to clearly distinguish the characteristic of each creep stage. Failure of the sample was dominated by the

Table 2: Viscoelastic parameter estimation results.

Number	G_K (MPa)	G_M (MPa)	η_K (GPa∗s)	η_M (GPa∗s)	Stress (MPa)	Condition
USN-1	807.2	67.3	$9.67E+11$	$1.07E+3$	20.3	Undamaged
USN-2	408.1	39.8	$6.70E+11$	$2.03E+4$	22.9	Damaged
USN-3	604.7	34.6	$1.73E+12$	$2.64E+4$	25.4	Damaged
USN-4	755.3	11.8	$3.11E+11$	$8.19E+4$	27.9	Damaged

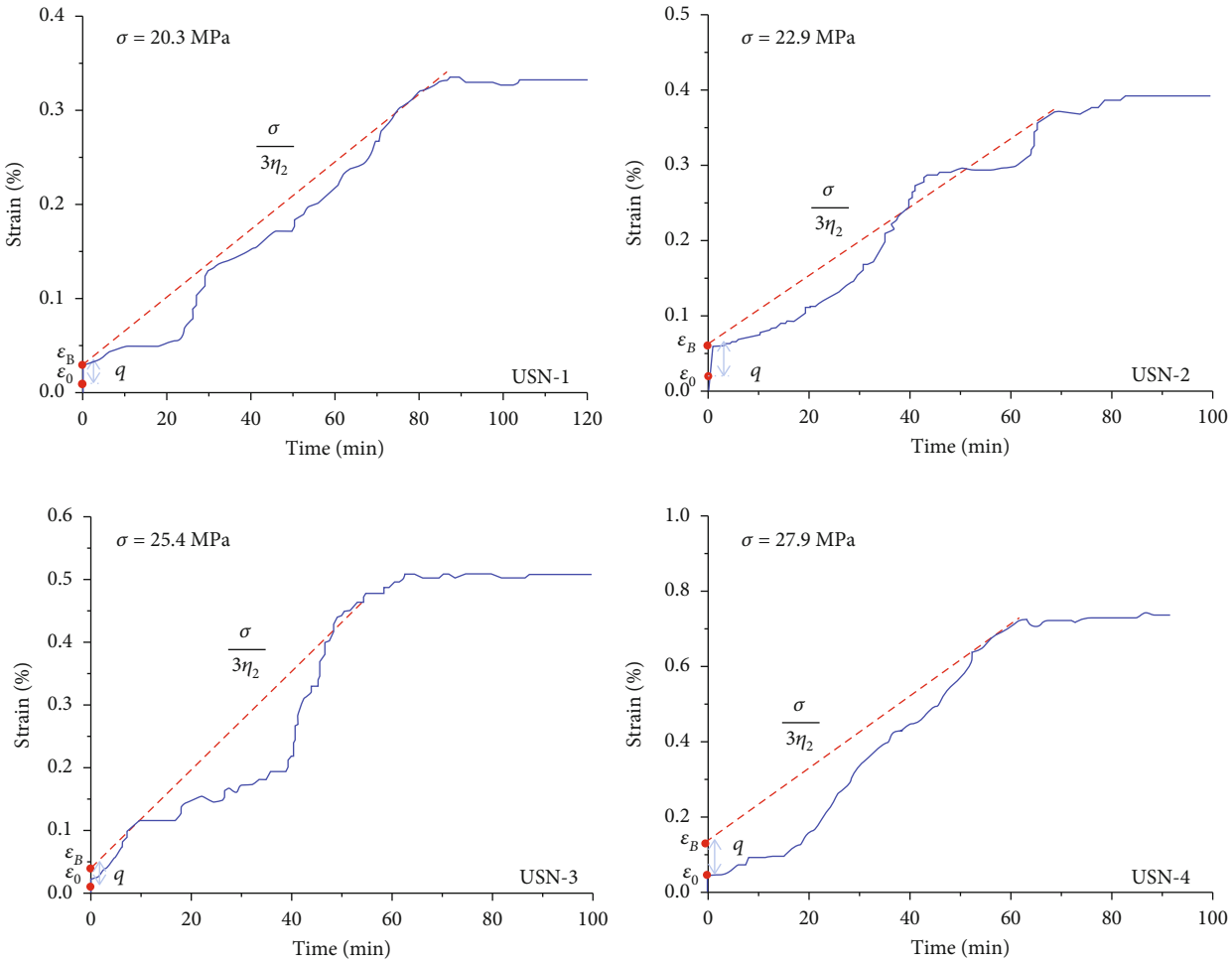

Figure 3: The axial strain-time curve of the USN rock samples.

horizontal and vertical cracks, and the horizontal and vertical penetrating cracks were generated simultaneously. The overall failure was relatively complete, and the residual strength was almost equal to zero. When USN-4 rock sample began to break, multidirection cracks were generated on the surface of the sample and continued to extend, accompanied by small and irregular rock fragments spalling, until the cracks were fully developed to penetrate the sample and resulted in complete failure. Failure of the sample was dominated by the transverse crack, and the failure part fell off from the sample along the transverse crack in a block shape. The damaged part of the sample was pulverized and had minimal residual strength.

To sum up, there was almost no anisotropic structure in USN rock samples, and the cracks did not generate or develop along a specific direction. The evolution path of crack generation, development, and final failure were random.

3.2. Discussion of the USN Rock Sample Parameters. In order to further study the response of nonstratified structural samples under constant load, we studied the viscoelastic parameters, analyzed the experimental data of the USN rock samples, and revealed the reasons why some rock samples did not fail.

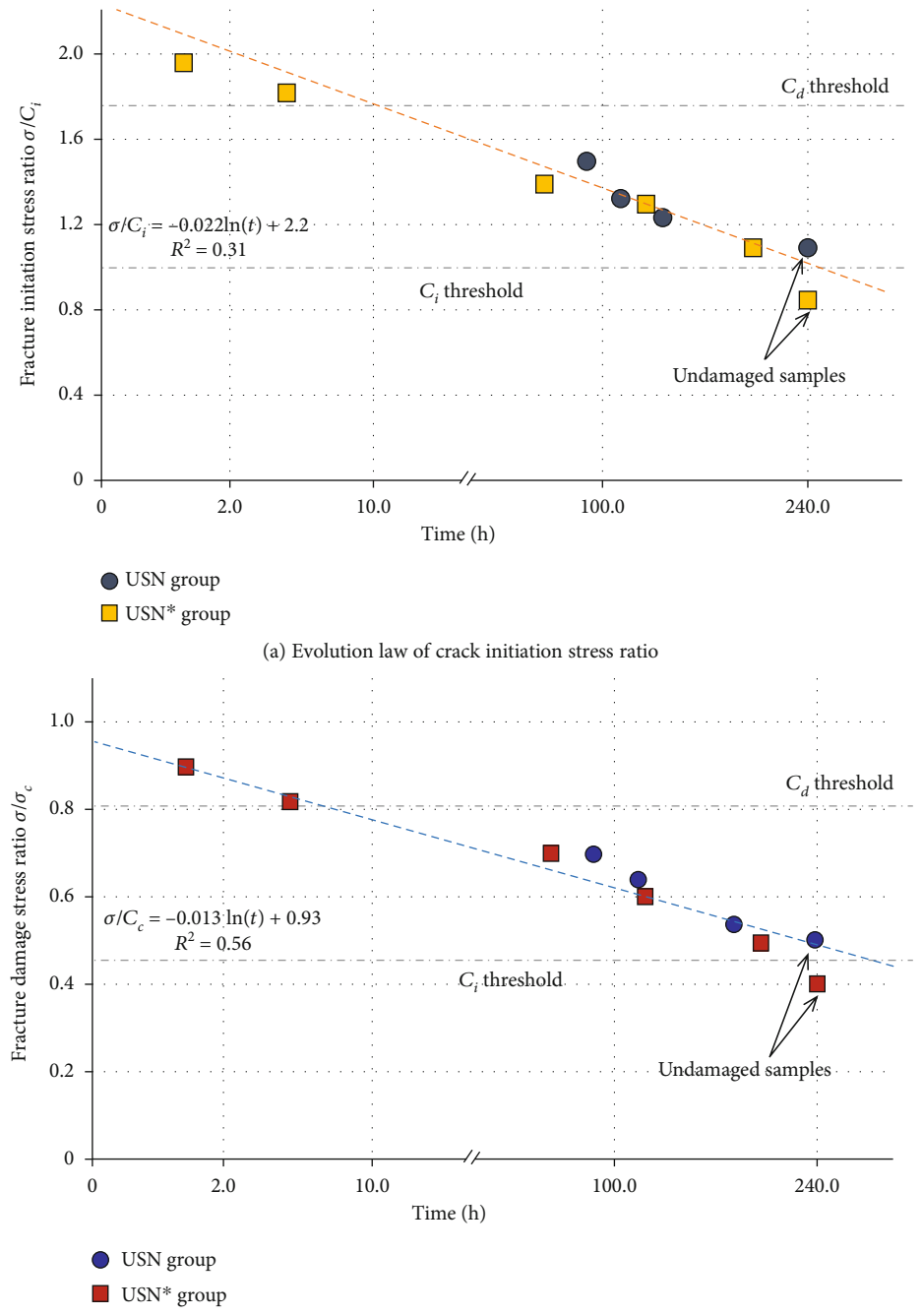

(a) Evolution law of crack initiation stress ratio

(b) Evolution law of crack damage stress ratio

Figure 4: Evolution law of constant load experiment parameters.

3.2.1. Discussion I: Viscoelastic Parameters of the USN Rock Samples. Viscoelastic parameters were estimated for all samples in the experiment. Kelvin shear modulus G_K, Maxwell shear modulus G_M, Kelvin viscosity η_K, and Maxwell viscosity η_M were obtained through parameter estimation (Table 2). In this study, the Goodman method was adopted to derive the parameters. Figure 3 shows the axial strain-time relationship curve obtained in the constant load experiment of the sample without stratified structure. The creep parameter estimation was based on the fitting of the Burgs model with experimental data, which could be achieved by plotting the asymptote of the constant strain rate stage or the secondary creep stage, then projecting it back to the time zero. And, because of the creep strain, based on the asymptote and the intercept of the strain axis, the axial strain at infinity (ε_B) can be estimated by parameters. Through the obtained parameters and constant load, Equation (1) to Equation (6) can be solved to obtain the viscoelastic

Table 3: Statistical results of constant load experimental parameters.

Sample number	Duration t (h)	Stress σ (MPa)	Crack initiation stress ratio (σ/C_i)	Crack damage stress ratio (σ/C_d)	Driving stress ratio (σ/σ_c)	Condition
USN-1	240.0	20.3	1.11	0.63	0.51	Undamaged
USN-2	120.3	22.8	1.24	0.70	0.57	Damaged
USN-3	108.7	25.4	1.38	0.78	0.63	Damaged
USN-4	94.2	27.9	1.52	0.86	0.70	Damaged
USN∗-1	240.0	16.1	0.87	0.50	0.40	Undamaged
USN∗-2	186.3	20.0	1.10	0.62	0.50	Damaged
USN∗-3	117.8	24.1	1.31	0.74	0.60	Damaged
USN∗-4	86.2	28.1	1.42	0.87	0.70	Damaged
USN∗-5	4.8	32.4	1.76	1.00	0.80	Damaged
USN∗-6	1.7	36.1	1.96	1.11	0.90	Damaged

parameters. The viscoelastic parameters obtained in this experiment are shown in Table 2.

$$\varepsilon_1(t) = \frac{2\sigma}{9K} + \frac{\sigma}{3G_M} + \frac{\sigma}{3G_K} - \frac{\sigma}{3G_K} e^{-((G_K/\eta_K)t)}, \quad (1)$$

$$\varepsilon_B = \sigma\left(\frac{2}{9K} + \frac{1}{3G_1} + \frac{1}{3G_2}\right), \quad (2)$$

$$\varepsilon_0 = \sigma\left(\frac{1}{9K} + \frac{1}{3G_2}\right), \quad (3)$$

$$\log q = \frac{-b \pm \sqrt{b^2 - 4ac}}{2a} \log\left(\frac{\sigma}{3G_1} + \frac{G_1}{3\eta_1}\right), \quad (4)$$

$$\frac{\sigma}{3G_2} = \varepsilon_B - \sigma\left(\frac{2}{9K} + \frac{1}{3G_1}\right), \quad (5)$$

$$K = \frac{\sigma}{3(\varepsilon_1 + 2\varepsilon_3)}, \quad (6)$$

where ε_1 is the axial strain; ε_3 is the radial strain; σ is the constant axial load; K represents the volume modulus; $\eta_1 = \eta_K$, where η_K is Kelvin viscosity coefficient; $\eta_2 = \eta_M$, where η_M is Maxwell viscosity coefficient; $G_1 = G_K$, where G_K is Kelvin shear modulus; $G_2 = G_M$, where G_M is Maxwell shear modulus; ε_0 is the instantaneous axial strain when a constant load is applied to the sample; and ε_B is the axial strain at an infinite distance along the time axis.

3.2.2. Discussion II: Comparative Analysis of the USN Rock Sample Experimental Data. In order to obtain the failure law of the USN rock samples and the difference of failure law with other types of rock, supplementary experiments were carried out. The sample number of the supplementary group was USN∗-1 to USN∗-6. Sampling sources, sampling standards, and physical and mechanical parameters of rock samples in this group were the same as those in the USN group. During the experiment, the load of $0.4\sigma_c$ to $0.9\sigma_c$ was applied to the six rock samples of the USN∗ group with a gradient of $0.1\sigma_c$. Crack initiation stress ratio and driving stress ratio were used to analyze the test results. The experiment results are shown in Figure 4. The data are from samples that were damaged during the experiment. We summarized the test results in Table 3; experiment data of the undamaged samples were included.

As can be seen from Table 3, when the constant load is greater than $0.8\sigma_c$, samples will be damaged within 2 hours. When the constant load is less than or close to the C_d threshold, the time required for samples to be damaged is longer, generally ranging from several days to one month.

3.2.3. Discussion III: Study on the Failure Cause of the USN Rock Samples. In order to study the causes of different failure states of samples under the same load conditions, the viscoelastic parameters obtained from each constant load experiment were correlated with the time t. Figure 5 shows that when G_K, η_K, and G_M are correlated with time, the failure of only a part of samples under the same load cannot be explained. However, from the perspective of parametric significance, since the Kelvin model describes delayed elasticity and Maxwell shear modulus refers to elastic shear modulus, both of which are almost independent of stress, so this result is predictable.

However, when the experimental data is correlated with Maxwell viscosity (η_M), a clear regularity appears between the two parameters, as shown in Figure 5(d). Maxwell viscosity describes the resistance of material to flow. The smaller the Maxwell viscosity is, the stronger its flow ability is, which is consistent with the results of this study. The results also show that samples with higher Maxwell viscosity are more prone to failure, while samples with lower viscosity tend to produce larger creep and failure in longer time domain due to its stronger flow ability.

It can be seen from Figure 5(d) that there exists a threshold value for Maxwell viscosity, below which rock samples produce creep that do not result in cumulative damage. To further explore the above finding, all the current experiment results were further examined, since the experiment study does not include the failure behavior and mechanism of rock samples under compressive stress less than the C_i threshold. Therefore, in the following study, a group of rock samples was added. The additional sample group was named as

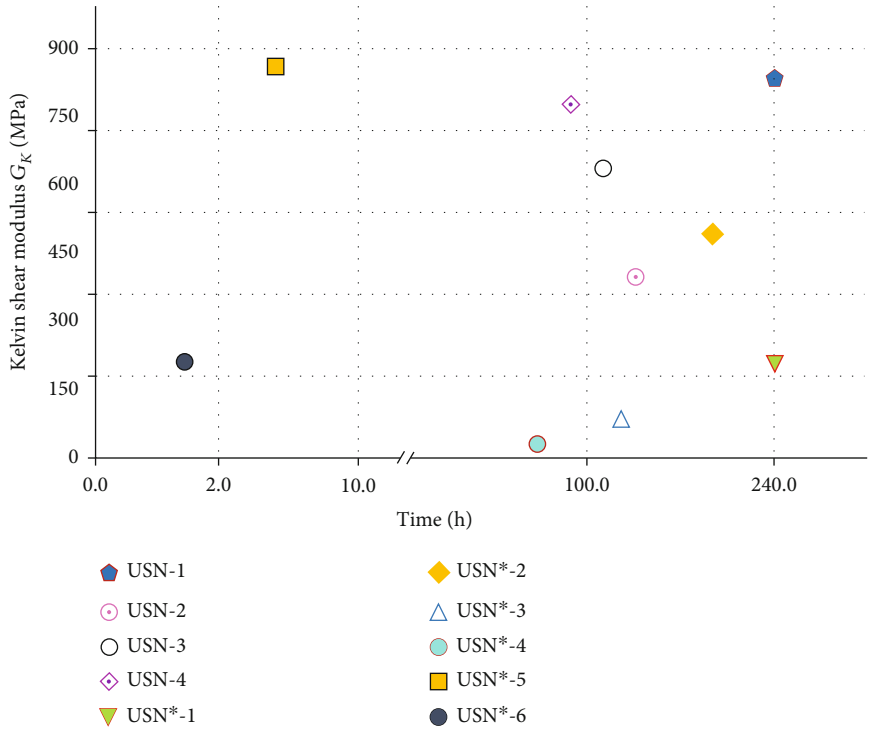

(a) Evolution of Kelvin shear modulus

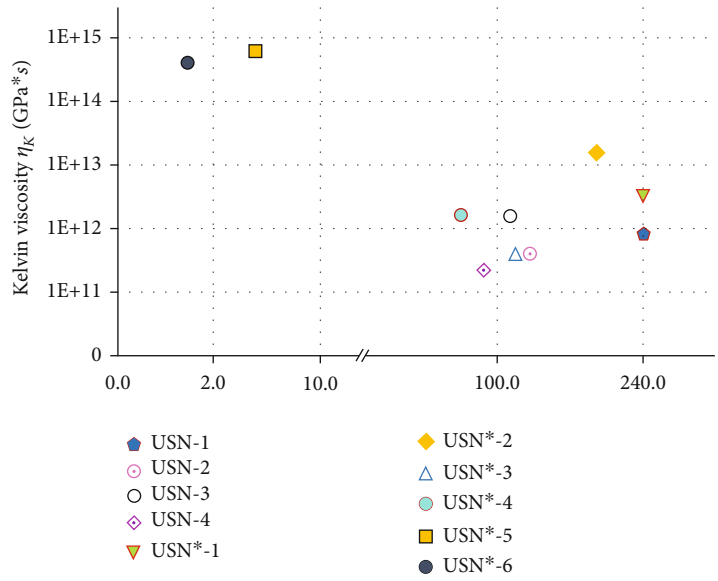

(b) Evolution of Kelvin viscosity

Figure 5: Continued.

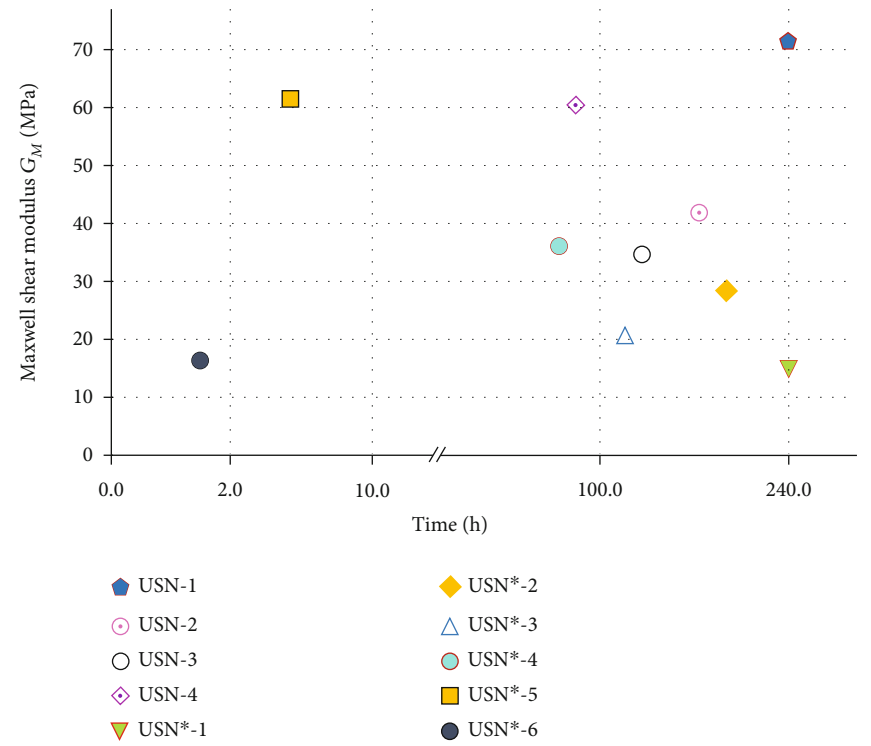

(c) Evolution of Maxwell shear modulus

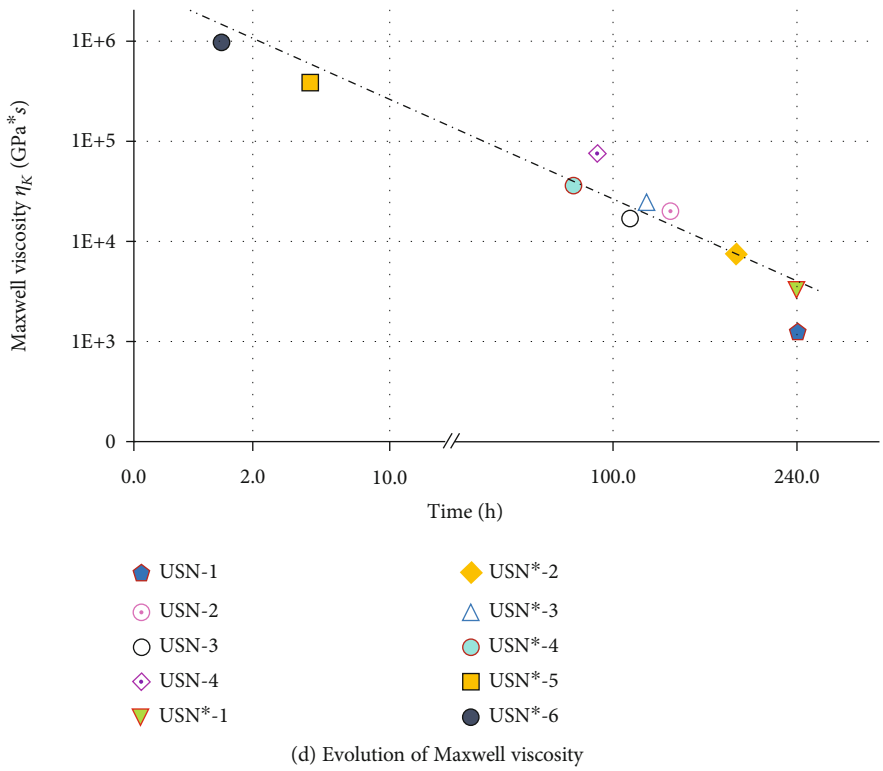

(d) Evolution of Maxwell viscosity

Figure 5: Evolution characteristics of viscoelastic parameters.

USN$^{\#}$, and the amount of samples is 5. Sampling sources, sampling standards, and physical and mechanical parameters of rock samples in this group were the same as those in the USN$*$ group. The samples were subjected to a constant load of $0.5C_i$, $0.6C_i$, $0.7C_i$, $0.8C_i$, and $0.9C_i$, respectively. The experiments ended with the failure or dead load time reaching 720.0 h (30 d). The results showed that when the constant load was greater than the C_d threshold, most of samples

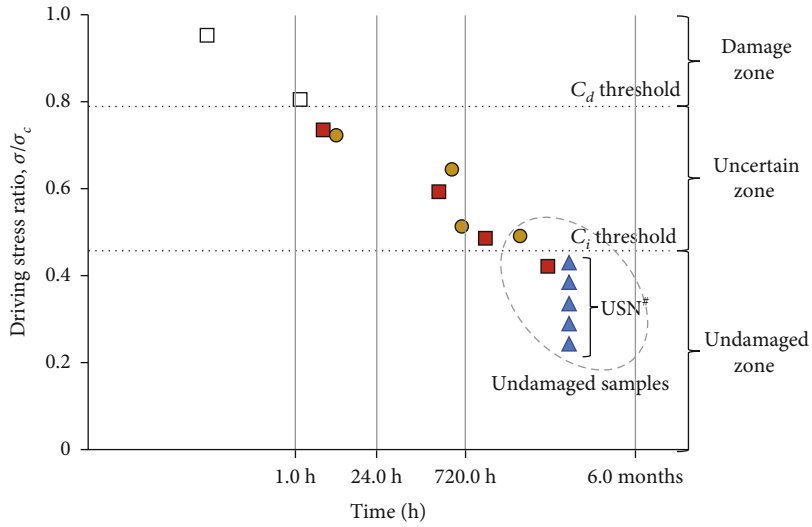

Figure 6: Comparison of experimental results.

failed within 24.0 hours due to the crack propagation and interaction. When the load was below the C_i threshold value, the native cracks inside the sample closed and were controlled by elastic strain, and the stress equilibrium state was established inside samples.

When the constant load is between the C_i threshold and the C_d threshold, as shown in Figure 6, this region is an uncertain region where damage occurs. This is because crack propagation and damage accumulation usually occur in a short period of time when the load is between the C_i threshold and the C_d threshold. But in the long run, as time goes on, the strength of the rock weakens, leading to its failure. However, there are some samples have not been damaged, and we believe that these cases can be explained with two reasons: The first one, there exists difference between internal structures of the selected samples and the normal sample, which leads to a sudden change of the strength and physical and mechanical parameters. The first one, the load on the samples is not maintained for enough time. Due to the historical and random nature of geological body, it is difficult to eliminate the internal structural differences of samples. Therefore, the abnormal samples should be adjusted from the aspect of optimizing the experiment time. Data from relevant scholars' literature indicate that failure is expected to occur when the time axis is extended long enough under a load close to $0.7\sigma_c$. Therefore, a test period of 3 months to 1 year should be planned in the later stage to check the mechanical behavior of samples under longer term load.

3.3. Experimental Result Analysis of Rock Samples from the USH Group. Constant load experiments were carried out on rock samples from the stratified structural rock sample groups. To simulate in situ stress caused by overburden geological body and tectonic stress in the natural environment, compressive load equivalent to 30%, 40%, 50%, 60%, 70%, 75%, 80%, and 85% of their uniaxial compressive strength was applied to rock samples.

Since the stress applied to the USH-1, USH-2, USH-3, and USH-4 rock sample was close to C_i threshold, the samples had certain elastic deformation at the initial stage. Both axial and radial strains increased, and the strain rate decreased at the end of the elastic deformation stage (Figure 7). When the elastic deformation stopped, the AE signal began to increase, which indicated that the native structures of the samples were damaged and new structures began to be generated. However, due to the fact that the constant load was close to C_i threshold, only a small part of weak structures inside the samples was damaged, and its contribution to the overall deformation of the samples was negligible. After elastic deformation and a small amount of plastic deformation, the samples began to enter the second creep stage. Due to the relatively low load, the samples only produced negligible deformation at the beginning of this stage and then entered the stress equilibrium state. Constant loads were maintained on the samples for about 150.0 h; the strain and AE parameters were kept a stable state, which indicated that the samples were completely in equilibrium and would not enter the third creep stage.

Since the load exerted on USH-5 to USH-8 sample was greater than the C_i threshold, and the load borne by some samples was even greater than the C_d threshold. The rock samples had undergone three typical creep stages. With the increase of load, the slope of time-strain curve increased; that is, with the increase of load, creep of the samples increased in per unit time. At the same time, with the increase of load, the failure time decreased and the final deformation increased. Failure modes of the samples were mainly vertical and oblique cracks which cut through the stratified structural plane, and the angle between the failure structural plane and the horizontal plane was generally greater than 45°. Among them, the USH-7 rock sample showed a lateral bulging failure pattern parallel to the horizontal structural plane. It was considered that the failure was caused by transverse extrusion of weak material between the horizontal structural

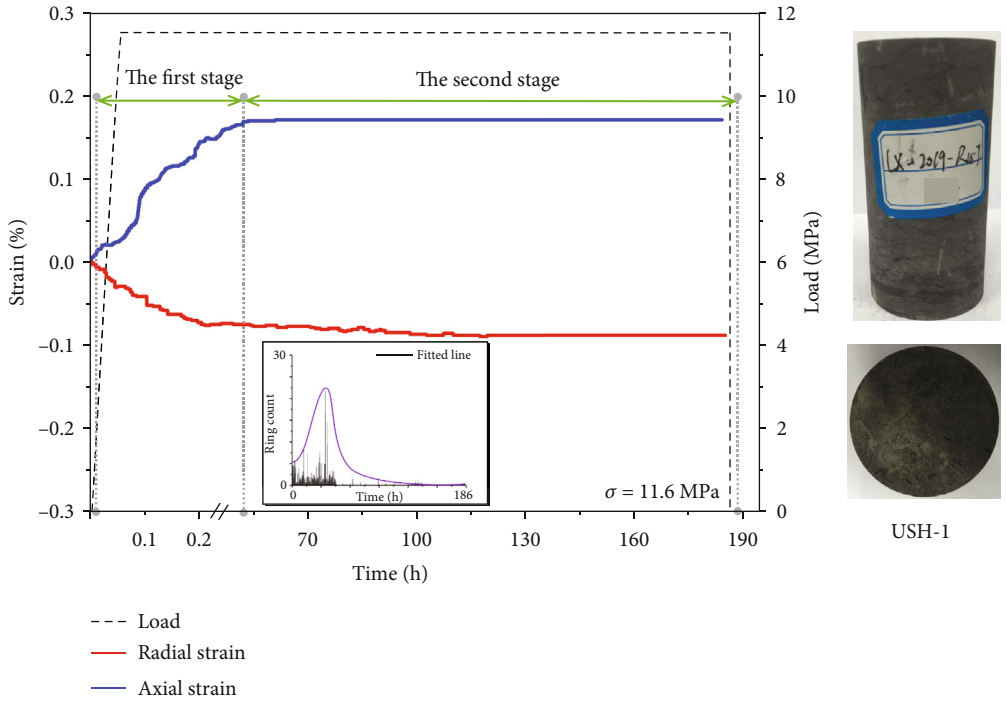

USH-1

(a) USH-1 sample

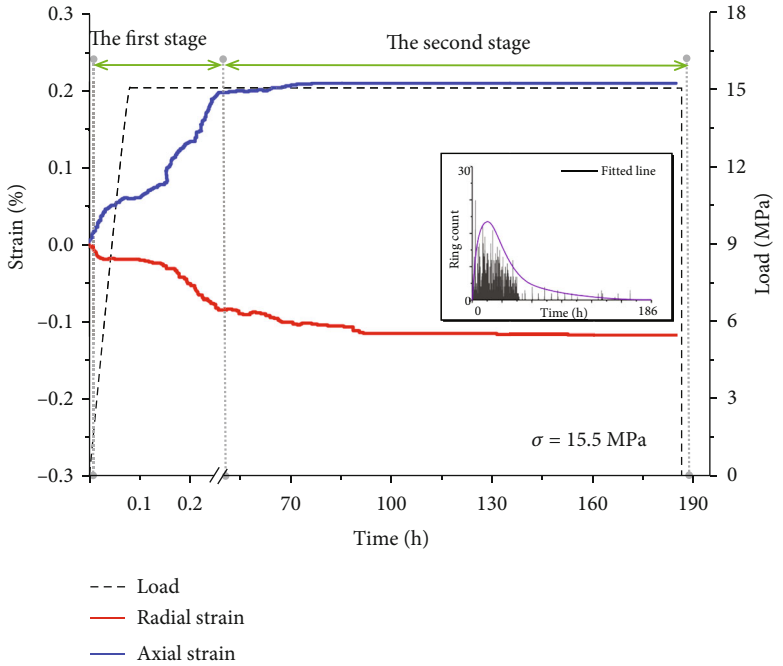

USH-2

(b) USH-2 sample

Figure 7: Continued.

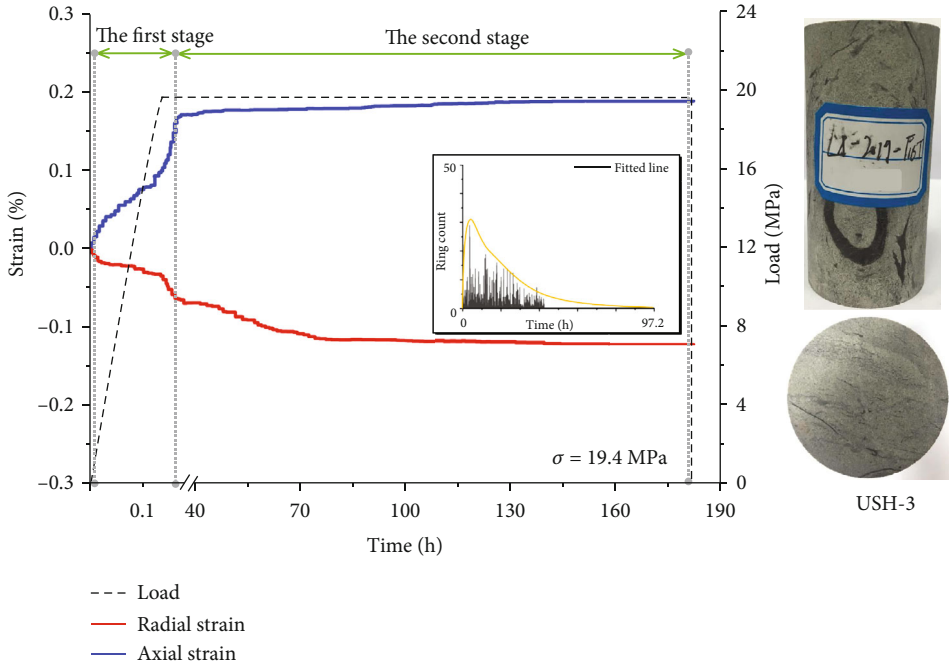

(c) USH-3 sample

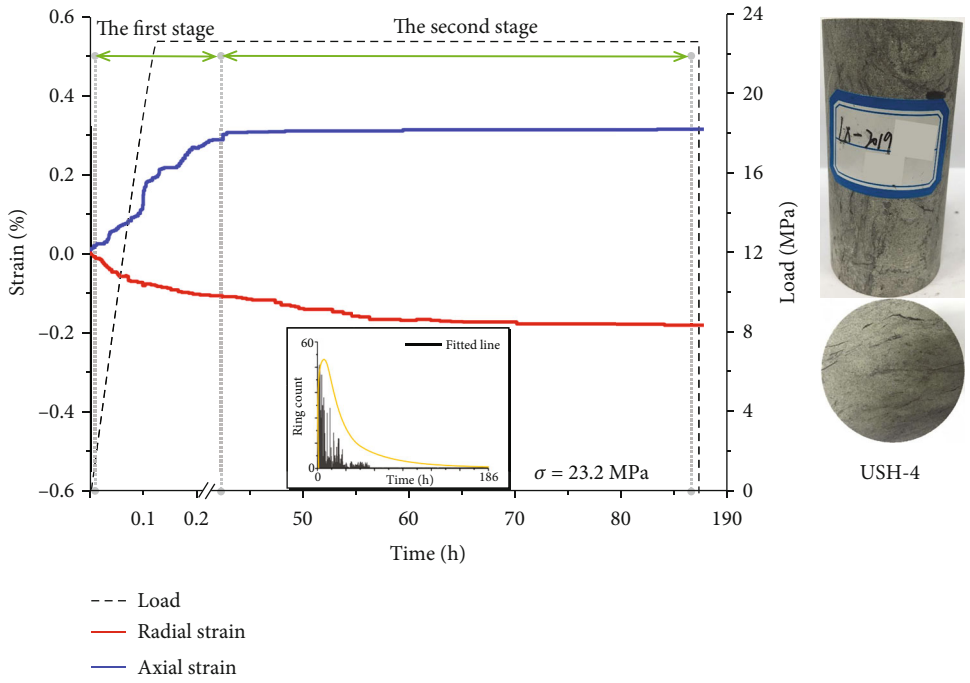

(d) USH-4 sample

Figure 7: Continued.

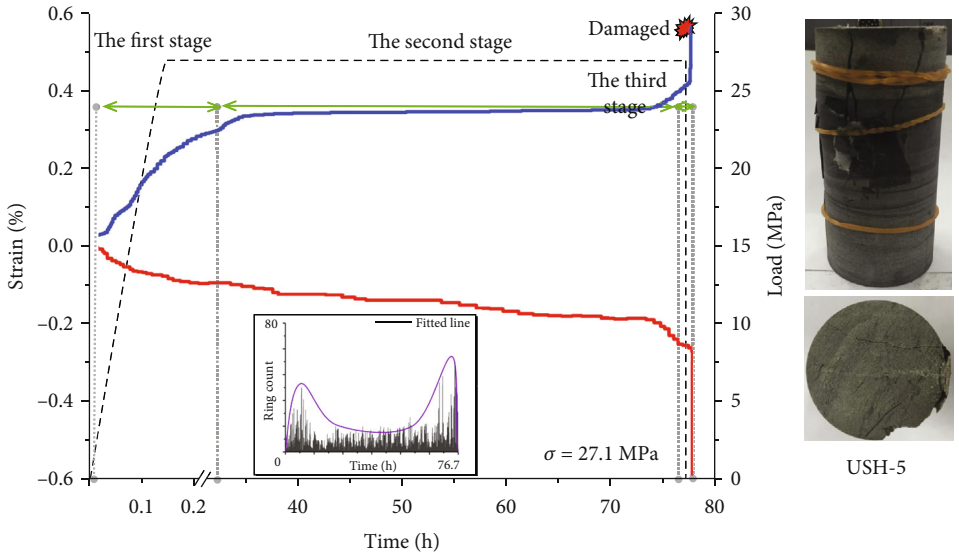

(e) USH-5 sample

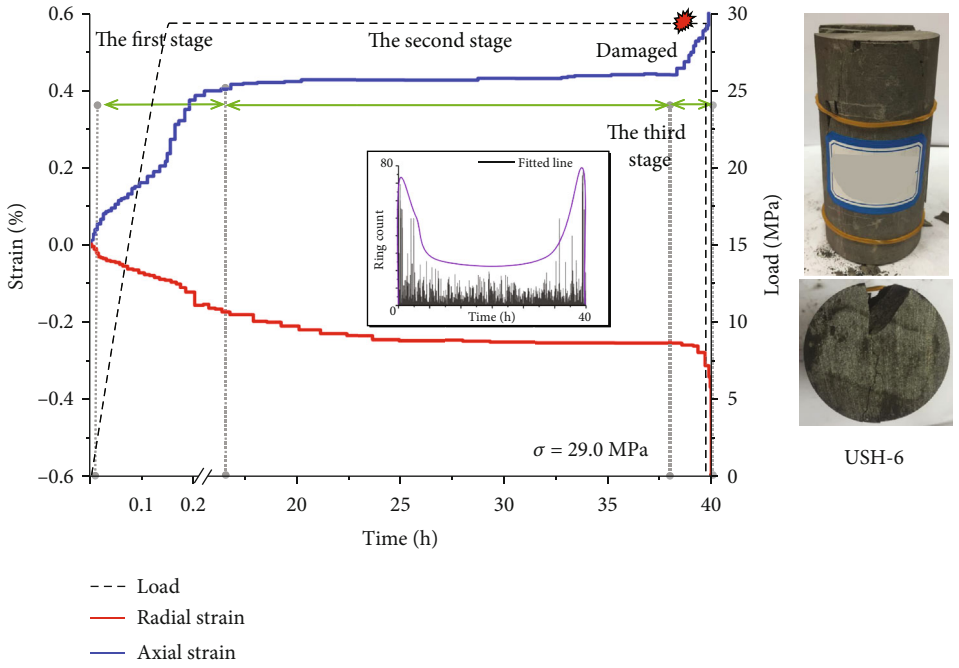

(f) USH-6 sample

Figure 7: Continued.

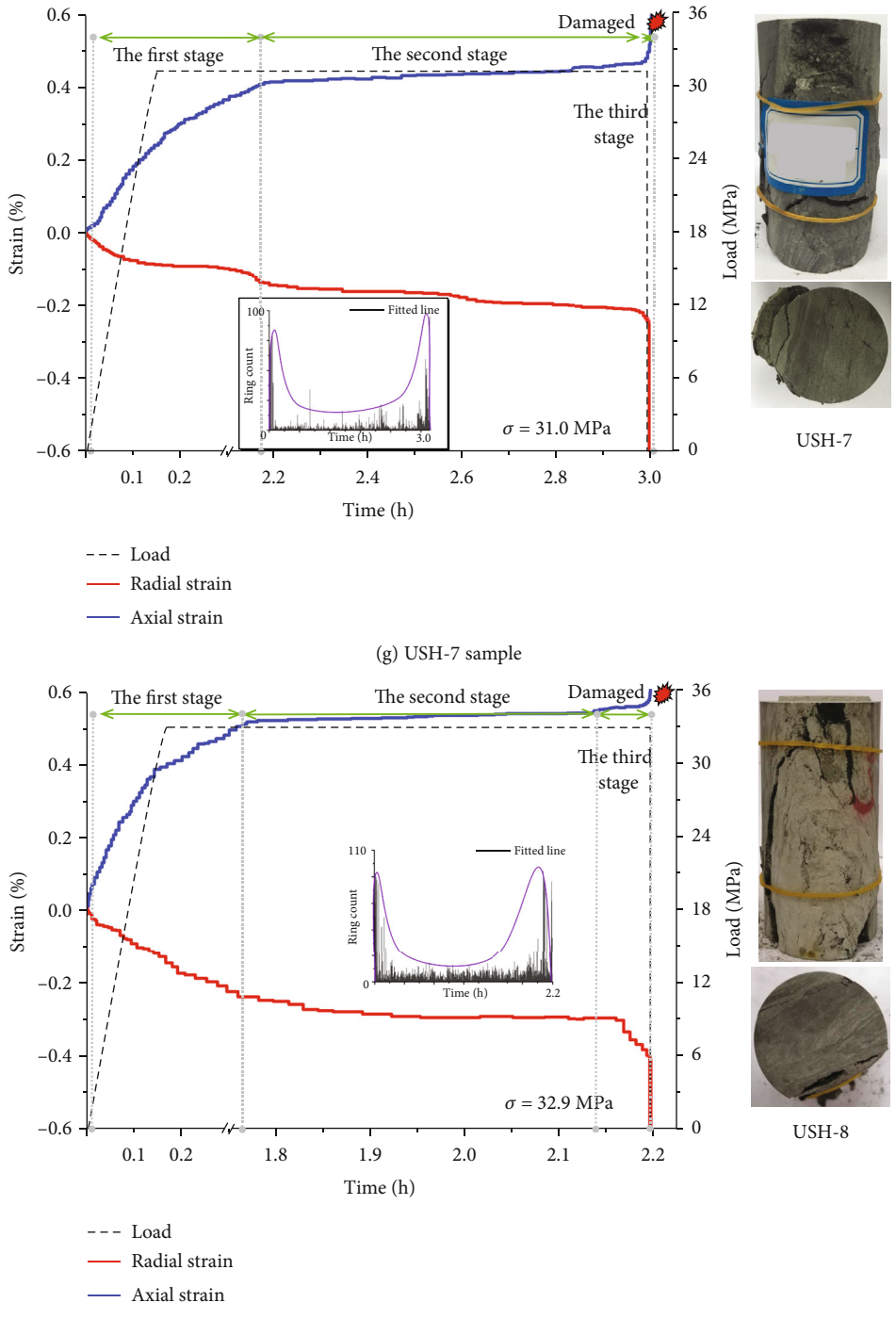

Figure 7: Constant load test curve of rock samples from the USH group.

planes under high load. Except for the semipenetrating failure surface of the USH-4 rock sample, the failure surfaces of the other samples all presented top-to-bottom penetrating failure. Therefore, the failure of USH samples usually require enough load to penetrate rock bedding. In general, the interbedding weak material does not play a decisive role in the failure mechanism of the USH samples, which is also the reason why the USH samples require greater load than the USO samples and the USV samples.

3.4. Experimental Result Analysis of Rock Samples from the USO Group. The loads exerted on the USO-1, USO-2, and USO-3 rock samples were all lower than the C_i threshold. After the first creep stage, the strain rate decreased, and the

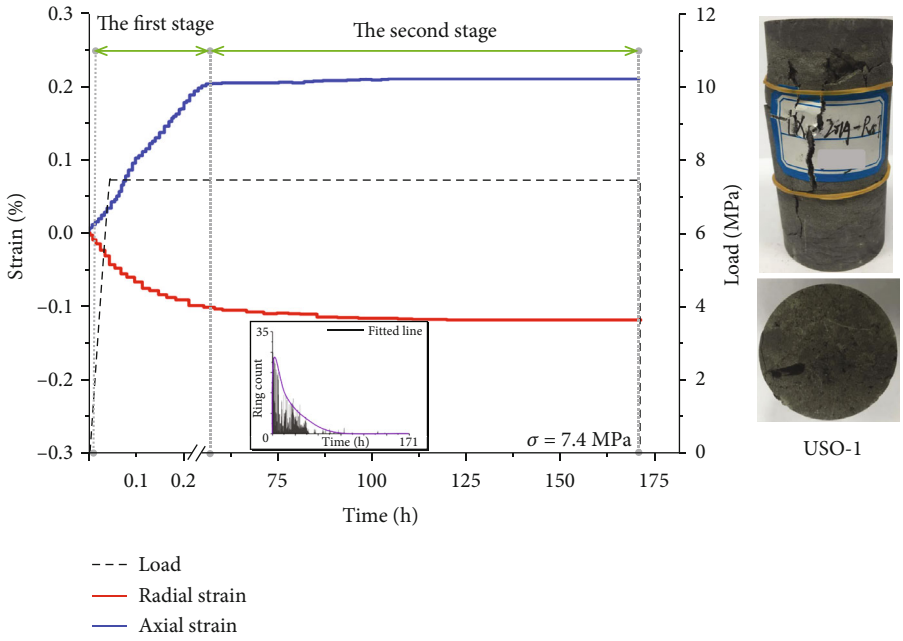

(a) USO-1 sample

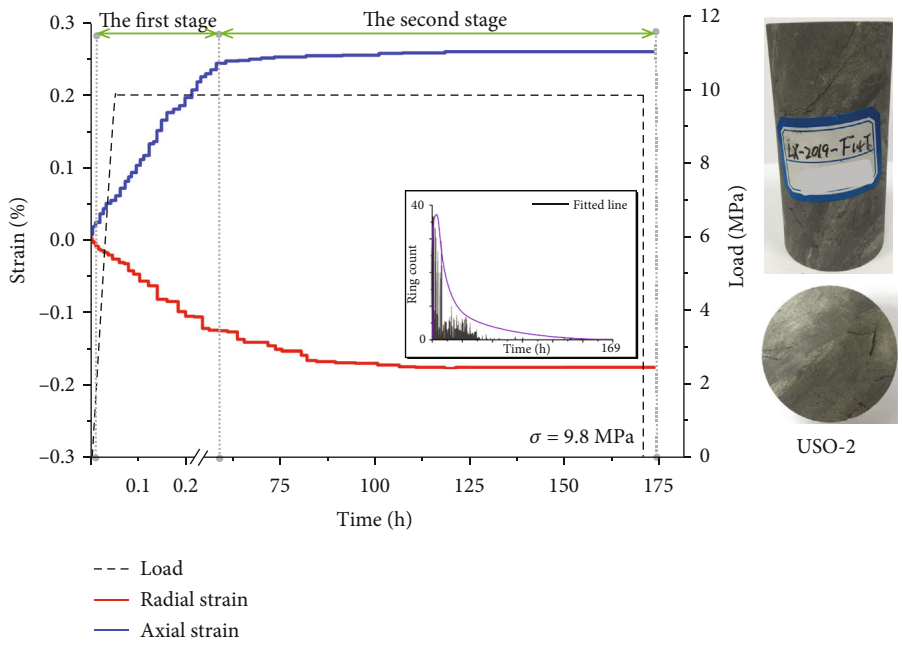

(b) USO-2 sample

Figure 8: Continued.

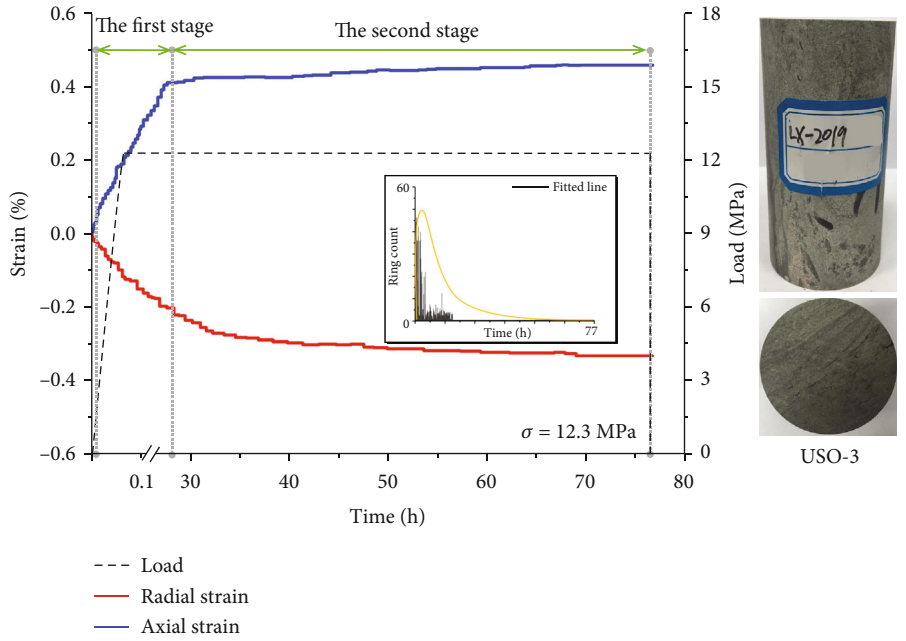

(c) USO-3 sample

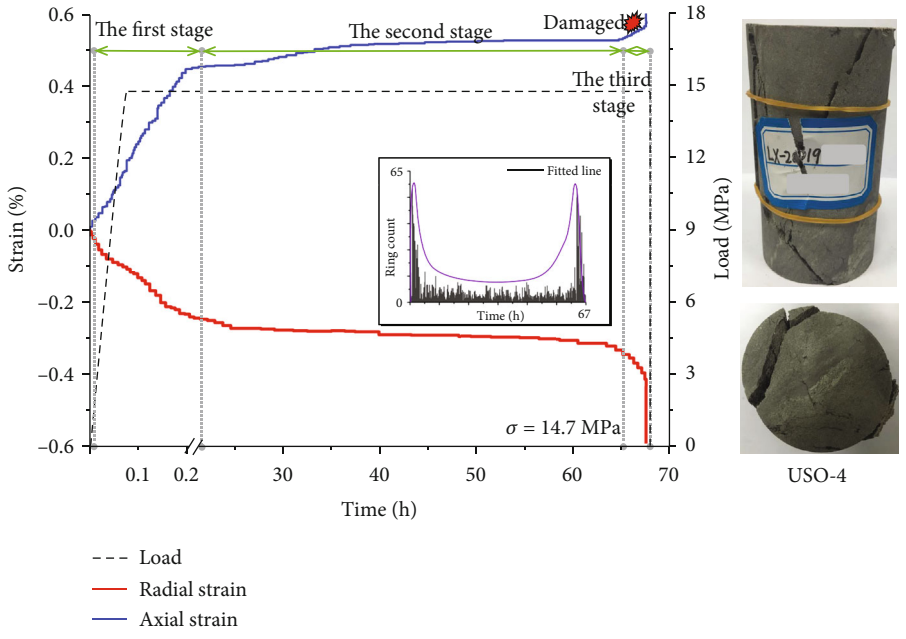

(d) USO-4 sample

Figure 8: Continued.

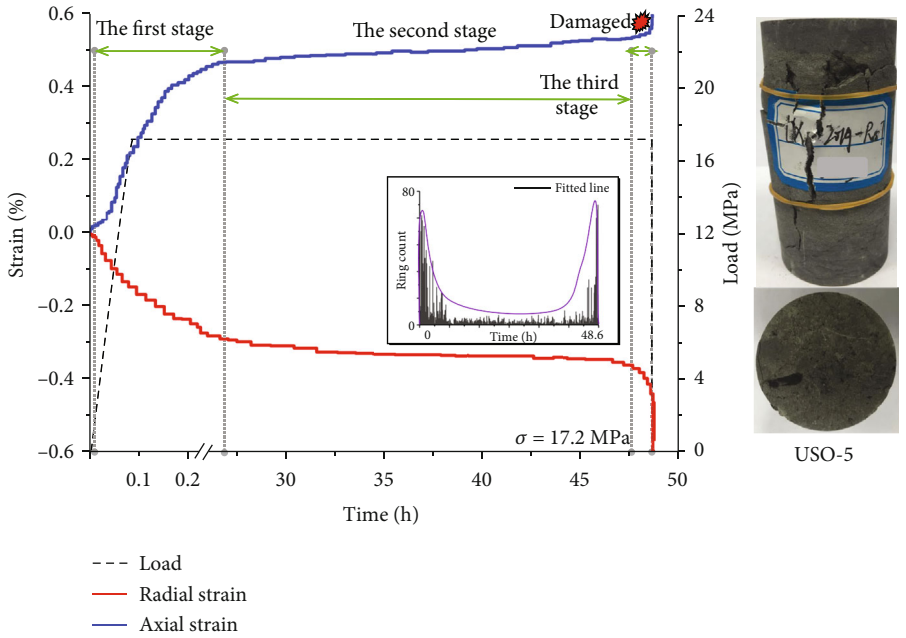

(e) USO-5 sample

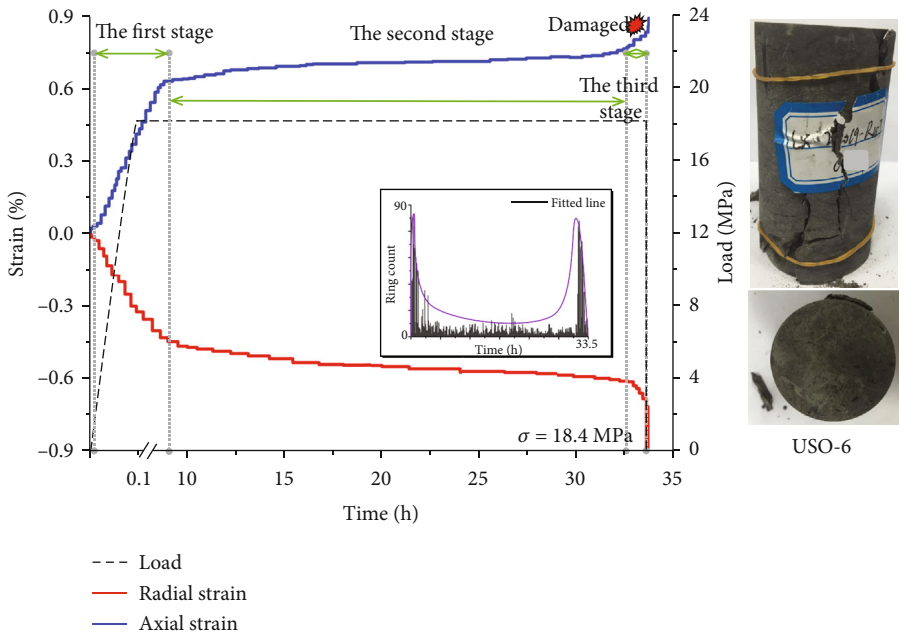

(f) USO-6 sample

Figure 8: Continued.

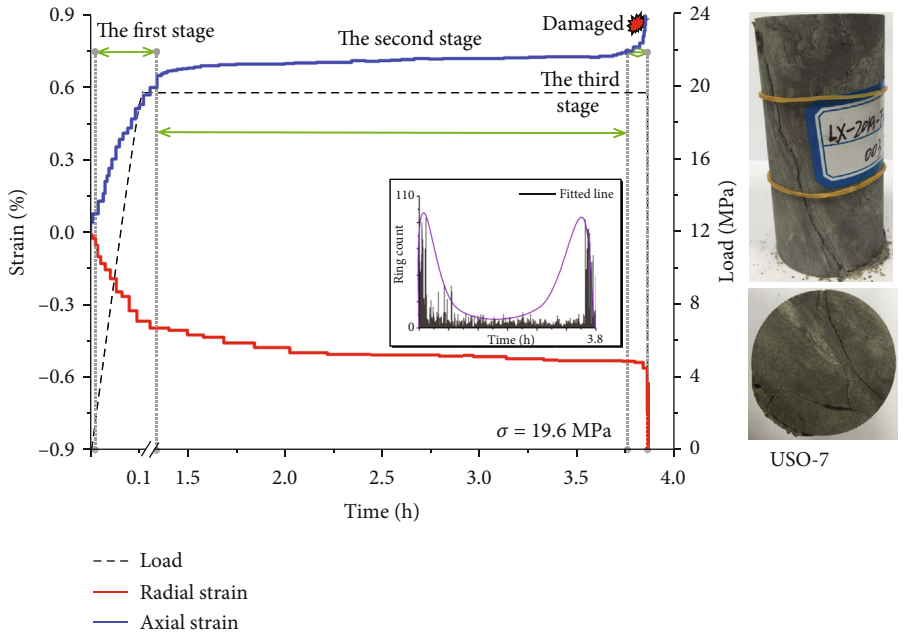

(g) USO-7 sample

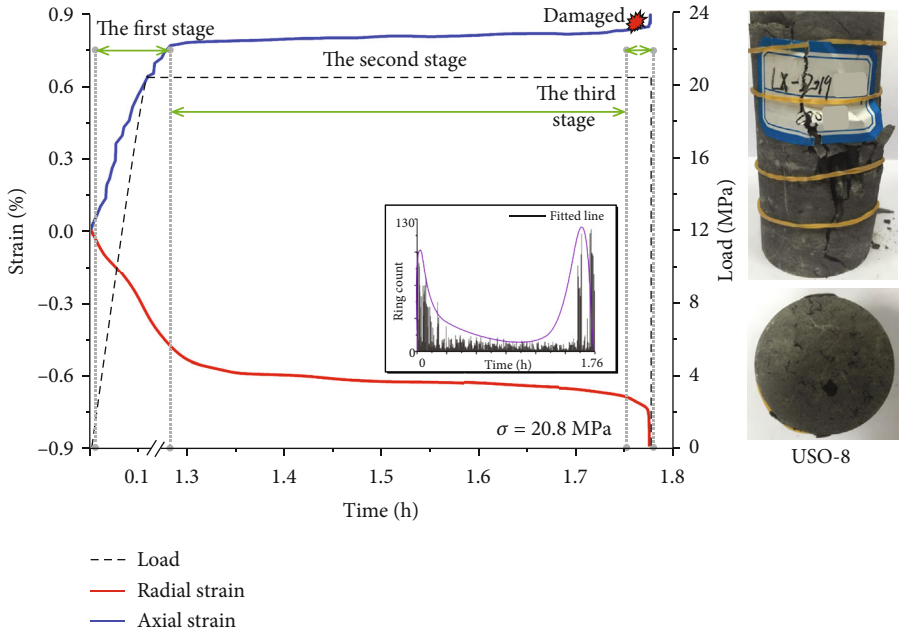

(h) USO-8 sample

Figure 8: Constant load test curve of rock samples from the USO group.

rock samples entered the second creep stage (Figure 8). Deformation rates of the rock samples tended to be zero and finally reached the stress equilibrium state. At this point, the change rate and the AE signals were both zero, indicating that the external deformation and the development of internal cracks of the samples were in a static state, which would not lead to the destruction of the samples.

The samples from USO-4 to USO-8 underwent three typical creep stages under the loads greater than the C_i threshold and the C_d threshold and finally failed. The duration of creep process was inversely proportional to the load; the final creep strain and the strain rate in the first creep stage were proportional to the load. The failure modes were mainly divided into two types, which were sliding along the structural plane and shear failure through the structural plane. Among them, the failure mode of USO-4 sample was a combination of the two types. When the load was large enough or there was a defect within the stratified structural plane, the failure path would develop along the weak material between bedding planes. It was also possible to break down the structural plane

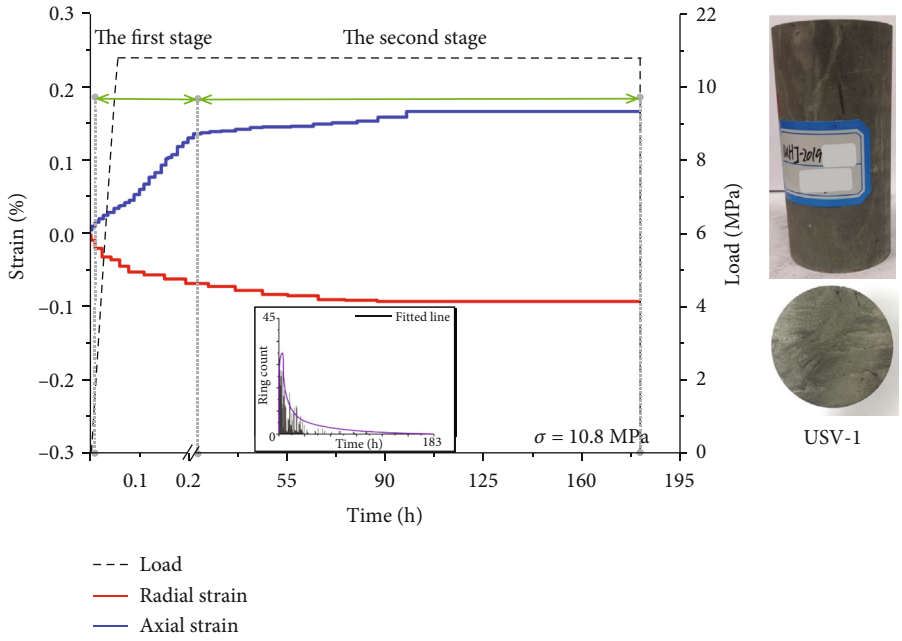

(a) USV-1 sample

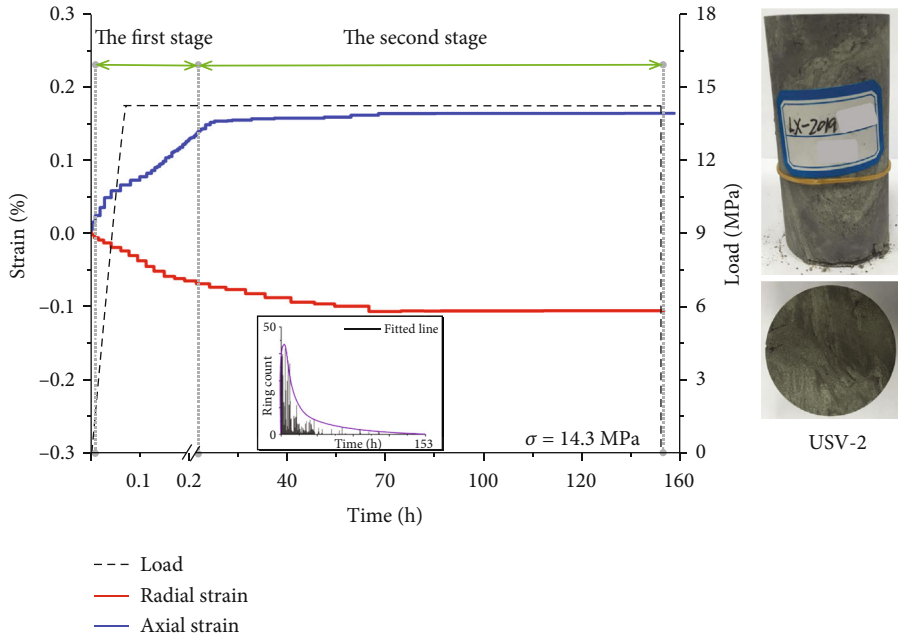

(b) USV-2 sample

Figure 9: Continued.

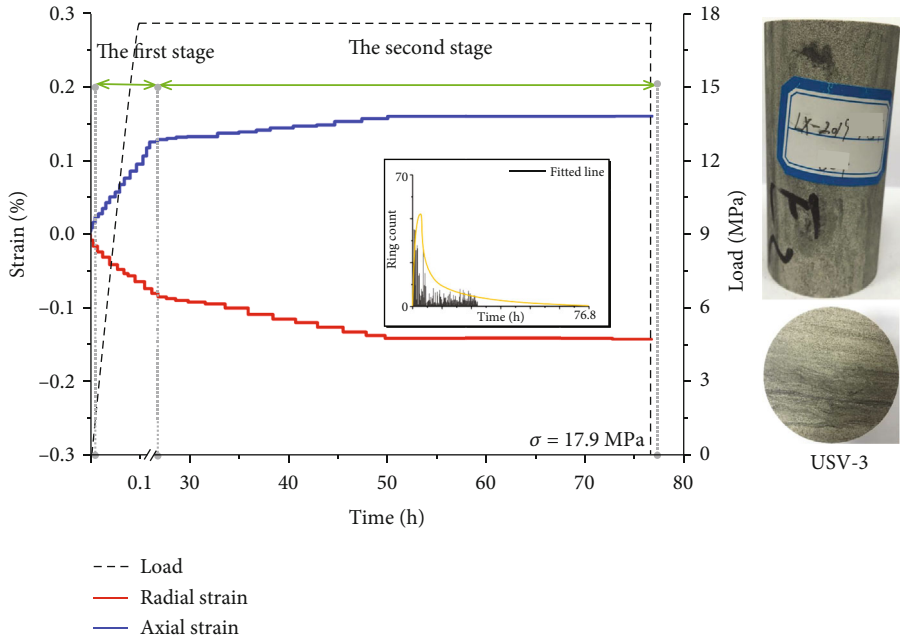

(c) USV-3 sample

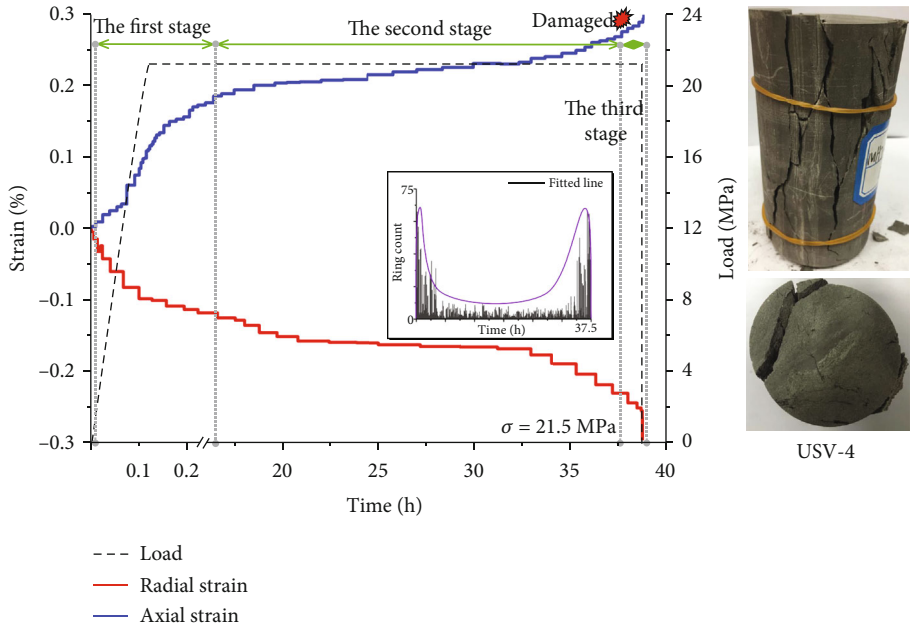

(d) USV-4 sample

Figure 9: Continued.

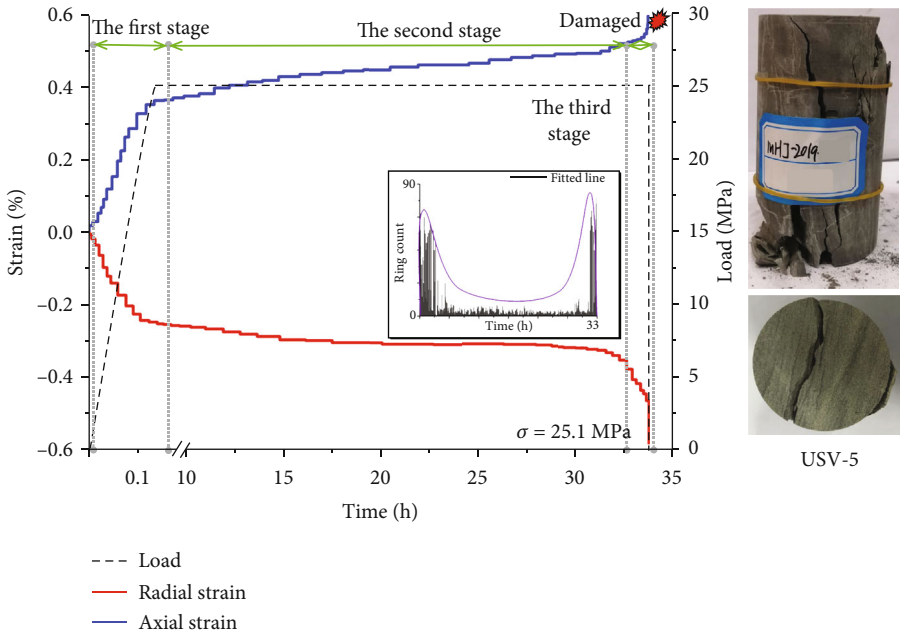

(e) USV-5 sample

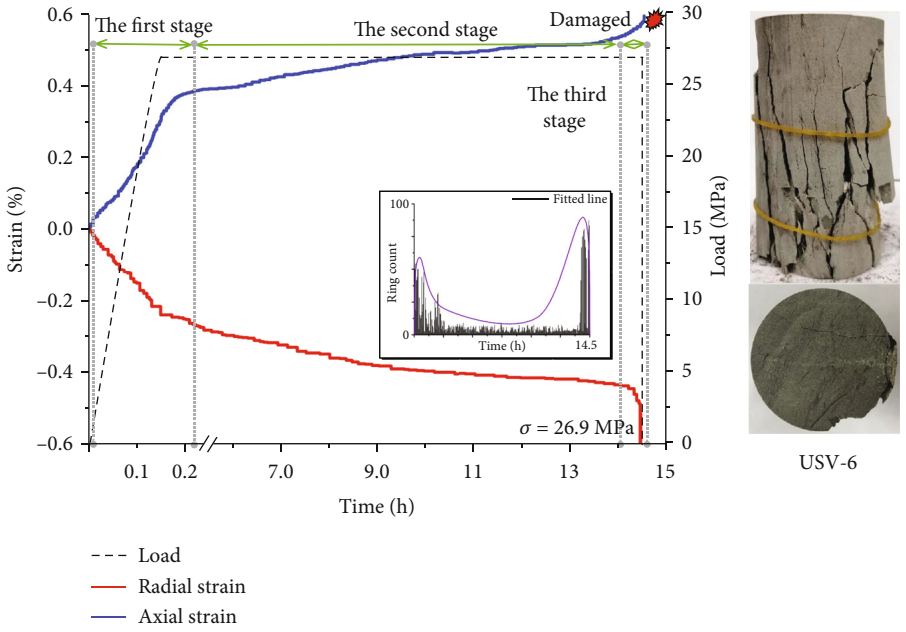

(f) USV-6 sample

Figure 9: Continued.

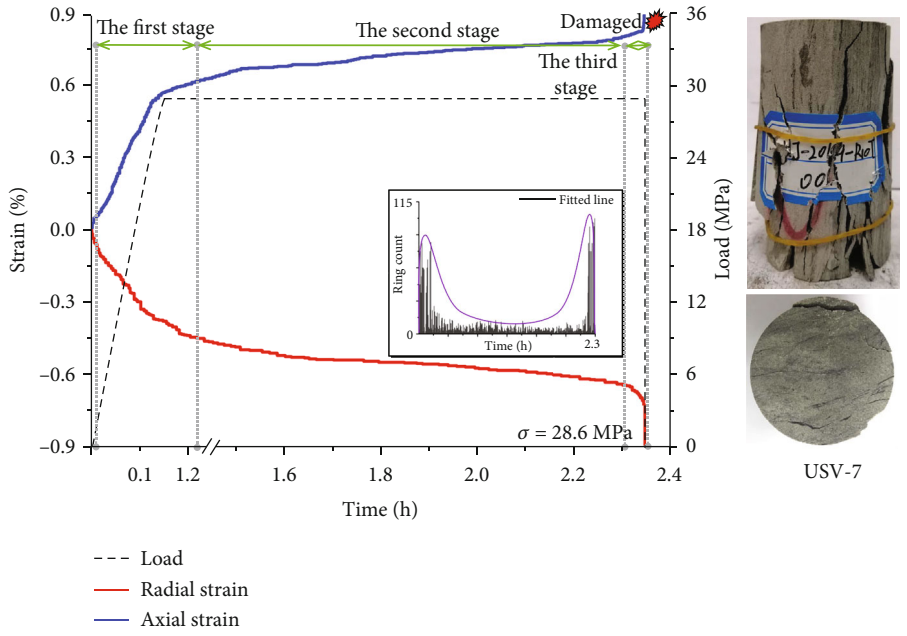

(g) USV-7 sample

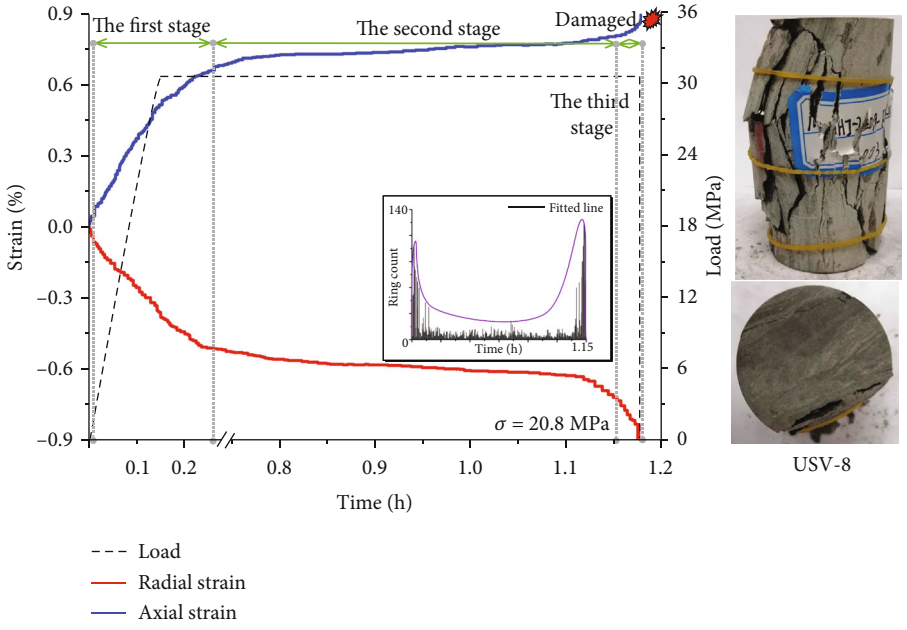

(h) USV-8 sample

Figure 9: Constant load test curve of rock samples from the USV group.

containing defects and then produce the combined failure mode. The failure mode of USO-7 sample was typical sliding failure along the structural plane, which was the main failure mode of USO samples. This was mainly due to the fact that failure path of the sample was preferred to develop along weak plane of the structure, while the material sandwiched between the stratified structural planes was usually argillaceous or argillaceous weak material, in which case the sample generally occurred sliding failure along the structural plane. The failure mode of USO-8 sample was the sliding failure along the structural plane, and the sliding failure part was in the form of transverse swelling and crack with the failure position at the center of this section. The main reason was that the rock mass was a plate-like structure; the structure was easy to produce transverse bulging and breaking failure in the direction of the free surface. This is very similar to the failure mechanism of deep tunnel.

3.5. Experimental Result Analysis of Rock Samples from the USV Group. USV-1 and USV-2 samples underwent the first

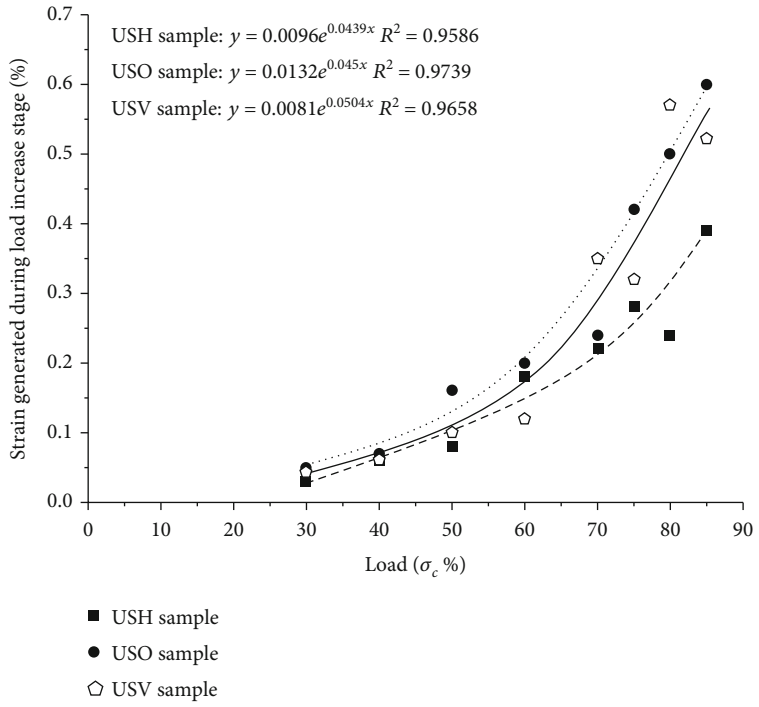

Figure 10: Relationship between strain and constant load in the stress increasing stage

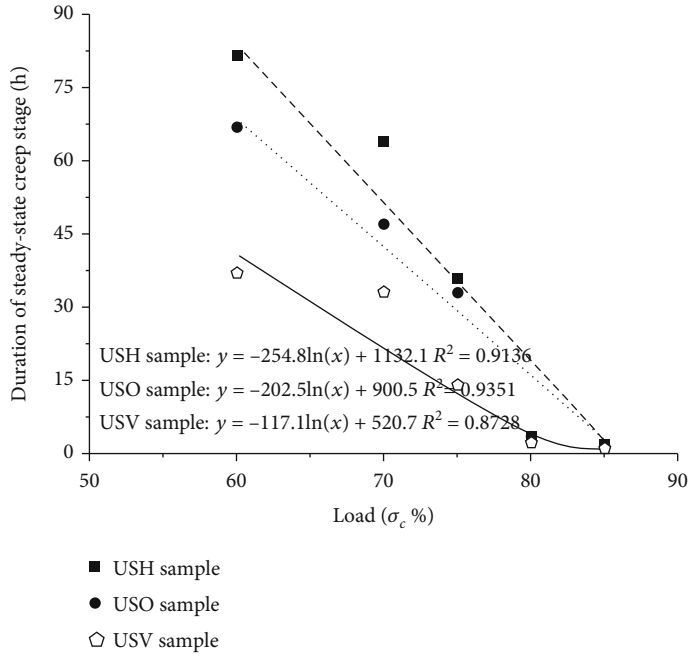

Figure 11: Relationship between duration of steady-state creep stage and constant load

and second creep stages under the constant load and finally reached the stress equilibrium state in the second creep stage (Figure 9).

The failures of USV-3 to USV-8 sample all went through three typical creep stages. The creep time was inversely proportional to the load; the final creep strain and the strain rate in the first creep stage were proportional to the load. Failure modes of the samples were mainly cross-layer shear failure along the structural plane and transverse shear failure along the normal direction of the structural plane. The specific failure process was as follows: under constant load, the stress state of the structural plane which was approximately perpendicular to the horizontal direction could be simplified to be the plate structure with fixed supports at both

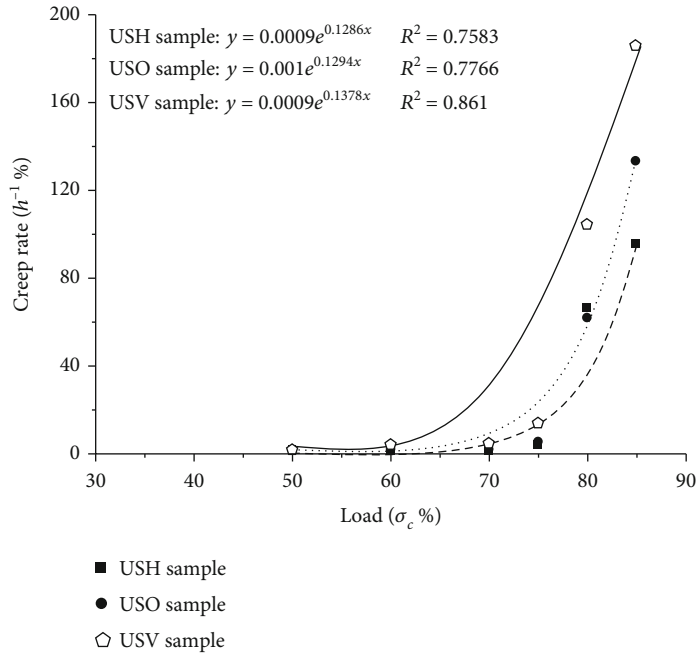

Figure 12: Relationship between creep rate and constant load of rock samples

ends. Under the disturbance of the horizontal component force, the transverse tension-shear failure occurred in the middle of the plate structure. In general, the stratified structure near the free surface without support broke first, and then the tension-shear failure occurred layer by layer from the outside to the inside until the sample was damaged completely.

It is worth noting that the failure modes of USV-6, USV-7, and USV-8 rock samples showed typical tension-shear failure from inside to outside layer by layer. The main difference was the position of the tension-shear failure. The tension-shear failure of bedding plane in the USV-6 rock sample was located at the lower position of the bedding plane, while the tensile shear failure of USV-7 and USV-8 rock samples was located in the middle and upper parts of the bedding plane. After the tensile shear failure occurred along the bedding plane layer by layer, the broken bedding plane fell off. The length of broken and exfoliated bedding surface decreased gradually from outside to inside, forming a horizontal conical cavity. At the upper and lower parts of the conical cavity, step-like rock steps were generated. The suspended inverted rock step located at the upper position could be simplified as a suspended plate structure with no constraint at the front end and fixed support at the back end. This kind of suspended plate structure was very likely to produce shear failure along internal structural plane and vertical shedding under gravity, which would cause significant hidden danger to safe construction.

3.6. Relationship among Creep Parameters. Strain-time curves of stratified rock samples have a nonlinear trend during stress increasing stage (Figure 10). The samples begin to deform when load is applied, and as the load gradually increases, the evolution of new cracks and the development of native cracks begin inside the samples. The effect of this process on the rheological parameters is significant. In this stage, deformation rates of the samples are an important index to measure the change state of their internal structure. The strain generated by the USH samples is the smallest while that of the USV samples is the largest in the process of load increase. This is caused by the induced tensile stress of horizontal bedding plane compression and the minimum strength in the tensile stress environment. Because the bedding planes in the USH samples are arranged along the direction of the minimum tensile stress and shear stress, the instantaneous strain is the smallest. The maximum instantaneous strain of the USO samples is caused by the bedding plane orientation close to the natural shear plane. The USV samples show intermediate instantaneous strain, which is caused by the decrease of the contact area between the samples and the press plate due to the crack sliding along the bedding plane. On the whole, strain is positively correlated with load in the process of load increase, and its evolution can be expressed as an exponential function relationship with base e, which is $\varepsilon_{in} = ae^{b\sigma}$.

$$\varepsilon_{in}^{H} = 0.0096e^{0.0439\sigma}, \quad (7)$$

$$\varepsilon_{in}^{O} = 0.0132e^{0.045\sigma}, \quad (8)$$

$$\varepsilon_{in}^{V} = 0.0081e^{0.0504\sigma}, \quad (9)$$

where ε_{in} is the strain generated during the load increase stage, σ is the load, and a and b are the coefficients. H, O, and V refer to three kinds of structurally anisotropic sandstones with horizontal, oblique, and vertical layered structures, respectively. The coefficient a ranges from 0.0081 to 0.0132, and the coefficient b ranges from 0.0439 to 0.0504.

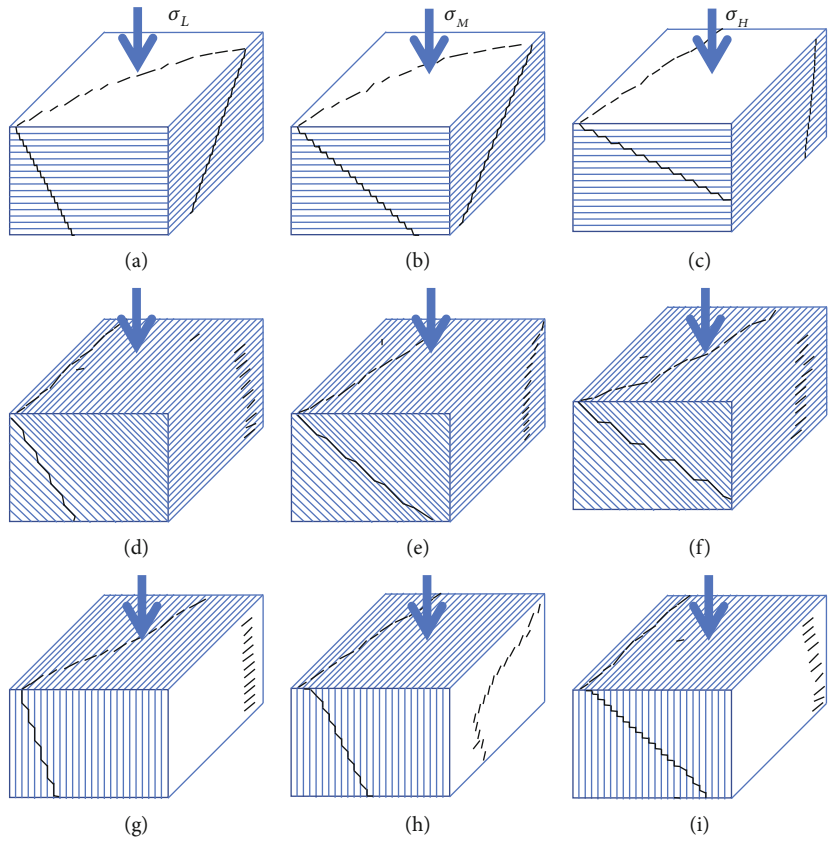

Figure 13: Characteristics of crack evolution in stratified rock mass.

The coefficient a of the USV samples is the minimum value of 0.0081, the coefficient a of the USH samples is the middle value of 0.0096, and the coefficient a of the USO samples is the maximum value of 0.0132. The coefficient b of the USV samples is the largest (0.0504), the coefficient b of the USO samples is in the middle (0.045), and the coefficient b of the USH samples is the lowest (0.0439).

The strain and duration of steady-state creep stage are important indexes to evaluate the mechanical properties of samples, so it is necessary to analyze and evaluate these two parameters for each sample. Under the influence of the native cracks parallel to the bedding, the USH samples have a small response to tensile stress. So the creep strain in the steady-state creep stage is the minimum. Under tensile stress perpendicular to the bedding plane, cracks, pore spaces, and openings exist along the bedding plane, which are the reasons for the large creep strain of the USV samples in the steady creep stage. The main reason for the medium creep strain of the USO samples in the steady creep stage is that the contact area between the samples and the machine tool pressure plate decreases due to the sliding and spalling of the samples layer by layer. There is a nonlinear negative correlation between the duration of steady-state creep stage and the load. It can be seen from the curve that, compared with the USV samples and the USO samples, the USH samples have the longest duration in the steady-state creep stage, followed by the USO samples, and the USV samples have the shortest duration. On the whole, the duration of steady-state creep stage decreases with the increase of load; it can be expressed as a logarithmic relationship, which is $t_s = a \ln \sigma + b$ (Figure 11).

$$t_s^H = -254.8 \ln \sigma + 1132.1, \tag{10}$$

$$t_s^O = -202.5 \ln \sigma + 900.5, \tag{11}$$

$$t_s^P = -117.1 \ln \sigma + 520.7, \tag{12}$$

where t_s is the duration of the steady-state creep stage and σ is the load. The duration of the steady-state creep stage decreases with the increase of the load, indicating that the influence of structural anisotropy on the duration of the steady-state creep stage decreases with the increase of the load. When the load reaches $0.8\sigma_c$ of the rock sample, the steady-state creep stage lasts for a short time, and the accelerated creep stage has a great influence on the deformation of the sample.

Due to the large creep caused by the stratified structure and the new anisotropic effect near the shear plane, it is found that before the failure of samples, the creep rate of the USV samples is the highest, and that of the USO samples is the second. This is due to the larger creep caused by the induced tensile stress perpendicular to the bedding in the USV rock samples. Due to the limited

effect of the induced tensile stress parallel to the bedding, the USH samples have the minimum creep rate. The relationship between the creep rate v_s and the load σ can be expressed as an exponential relationship base e, which is $v_s = ae^{b\sigma}$ (Figure 12).

$$v_s^{\mathrm{H}} = 0.0009e^{0.1286\sigma}, \tag{13}$$

$$v_s^{\mathrm{O}} = 0.001e^{0.1294\sigma}, \tag{14}$$

$$v_s^{\mathrm{V}} = 0.0009e^{0.1378\sigma}, \tag{15}$$

where v_s is the creep rate and σ is the load. The USV samples have the highest creep rate, followed by the USO samples, and the USH samples have the lowest creep rate. On the whole, when the constant load is less than $0.75\sigma_c$, creep rates of the three groups are almost the same. When the stress is greater than $0.80\sigma_c$, the creep rates are different due to the inherent anisotropy. This phenomenon indicates that the stratified structure in the sample has a great influence on the creep rate under high load.

For the USH samples, the shear crack array produces the minimum tensile stress and shear stress along the bedding plane perpendicular to the stress axis. With the increase of load, slanted wing cracks are generated on the basis of the original crack array. An array of shear cracks is formed in the USH group samples; tensile crack arrays are formed in the USO group samples and in the USH group samples. But the length is shorter in the USH samples. Under lower load, due to the difference of the steady-state creep rate, the tensile crack array length of the USV samples is the longest, and that of the USH samples is shorter, while that of the USO samples is the shortest. With the increase of load, the tensile crack array becomes shorter and the shear crack array becomes longer. Finally, the shear crack independent of the anisotropy of the structure is generated. The difference of instantaneous strain of various rock samples is due to the fact that no crack comes into being, and the deformation type is limited to elastic deformation. It can be inferred that the stratified structure has obvious influence on the instantaneous strain of the samples. Similarly, the gradual reduction of the deceleration creep stage also can be explained by the concept of the cascade crack arrangement theory.

The opening stage of natural cracks and pore space in the stratified sandstone dominate the structural anisotropy under low load. However, under high load, the opening stage of inherent cracks and pores is not strictly controlled by structural anisotropy. Therefore, the structural anisotropy loses its control over deformation and the rock samples behave mechanically as an isotropic material. The microstructure makes the rock break through the elastic limit through the change of load from low to high. And the creep stage of the auxiliary activated rock is directly transferred to the steady creep stage and the accelerated creep stage, without the deceleration creep stage. Due to the influence of the above processes, the creep behavior of rock is eventually transformed into a short-term monotone deformation (Figure 13). This deformation makes rock intrinsically more fragile. Therefore, because the three groups of structural anisotropic rock samples all generate shear crack arrays directly, structural anisotropy has a weak or even negligible control over deformation. With the influence of the new anisotropy (cracks and fissures), the sample exhibits the steady creep strain after the elastic deformation. From the concept of step crack array, rock creep under low load is the result of nucleation and propagation of step crack array. However, under high load, the shear crack array is not controlled by structural anisotropy. All the three groups of rock samples show shear failure has little correlation with the anisotropy of rock.

4. Conclusions

(1) The evolution path of crack generation, development, and final failure of the USN samples is random. This is because there is no obvious anisotropic structure in the USN samples, so the failure does not occur along a specific structural path. The failure mode of the USH samples is mainly splitting failure, and the crack plane penetrates the stratified structure plane vertically and obliquely. The failure modes of the USO samples mainly behave as slip failure along the structural plane and shear failure through the structural plane. The failure modes of the USV samples mainly behave as bedding shear failure along a structural plane and transverse bulging shear failure along the normal direction of a structural plane

(2) The creep curves of these three types of stratified structural samples are nonlinear. The evolutionary relationship between instantaneous strain generated in the stress increasing stage and the load can be expressed as an exponential function base e, $\varepsilon_{\mathrm{in}} = ae^{b\sigma}$. The relationship steady-state creep stage duration and the load can be expressed as logarithmic function, $t_s = a \ln \sigma + b$. The relationship between the creep rate and the load can be expressed as an exponential function base e, $v_s = ae^{b\sigma}$

Data Availability

The data used to support the findings of this study are currently under embargo while the research findings are commercialized. Requests for data, 18 months after publication of this article, will be considered by the corresponding author.

Conflicts of Interest

The authors declare that there is no conflict of interest regarding the publication of this paper.

Acknowledgments

This work was supported in part by the Scientific Research Project of Shaanxi Provincial Department of Education under grant No. 21JK0952, in part by the High-Level Talents Special Fund of Xijing University under grant No. XJ21B12, and in part by the Key National Natural Science Foundation of China under grant No. U1361206. The authors are grateful to China Scholarship Council (CSC). Special thanks are due to Professor Pinnaduwa. H.S.W. Kulatilake, Department of Mining and Geological Engineering, the University of Arizona, Tucson, AZ, USA.

References

[1] J. Barlow, "Rock creep and the development of the Niagara Cuesta," *Earth Surface Processes and Landforms*, vol. 27, no. 10, pp. 1125–1135, 2002.

[2] V. Karev, D. Kilmov, Y. Kovalenko, and K. Ustinov, "Experimental study of rock creep under true triaxial loading," *Mechanics of Solids*, vol. 54, no. 8, pp. 1151–1156, 2019.

[3] Y. Yang, X. Lai, T. Luo, K. Yuan, and F. Cui, "Study on the viscoelastic–viscoplastic model of layered siltstone using creep test and RBF neural network," *Open Geosciences*, vol. 13, no. 1, pp. 72–84, 2021.

[4] E. Zha, Z. Zhang, R. Zhang et al., "Long-term mechanical and acoustic emission characteristics of creep in deeply buried jinping marble considering excavation disturbance," *International Journal of Rock Mechanics and Mining Sciences*, vol. 139, p. 104603, 2021.

[5] H. Wu, D. Ma, S. Spearing, and G. Zhao, "Fracture phenomena and mechanisms of brittle rock with different numbers of openings under uniaxial loading," *Geomechanics and Engineering*, vol. 25, no. 6, pp. 481–493, 2021.

[6] H. Wu, B. Dai, L. Cheng, R. Lu, G. Zhao, and W. Liang, "Experimental study of dynamic mechanical response and energy dissipation of rock having a circular opening under impact loading," *Mining, Metallurgy & Exploration*, vol. 38, no. 2, pp. 1111–1124, 2021.

[7] X. Shi, C. Zhao, C. Li, and D. Wen, "Experimental study on rock creep fracture and its load/unload response ratio," *Acta Seismologica Sinica*, vol. 32, pp. 332–339, 2010.

[8] D. Park and R. Michalowski, "Roof stability in deep rock tunnels," *International Journal of Rock Mechanics and Mining Sciences*, vol. 124, p. 104139, 2019.

[9] L. Liu, G.-m. Wang, J.-h. Chen, and S. Yang, "Creep experiment and rheological model of deep saturated rock," *Transactions of Nonferrous Metals Society of China*, vol. 23, no. 2, pp. 478–483, 2013.

[10] R. K. Dubey and V. K. Gairola, "Influence of structural anisotropy on creep of rocksalt from Simla Himalaya, India: an experimental approach," *Journal of Structural Geology*, vol. 30, no. 6, pp. 710–718, 2008.

[11] S. Zivaljevic and Z. Tomanovic, "Experimental research of the effects of preconsolidation on the time-dependent deformations—creep of marl," *Mechanics of Time-Dependent Materials*, vol. 19, no. 1, pp. 43–59, 2015.

[12] F. Pellet and G. Fabre, "Damage evaluation with P-wave velocity measurements during uniaxial compression tests on argillaceous rocks," *International Journal of Geomechanics*, vol. 7, no. 6, pp. 431–436, 2007.

[13] S. Rahimi and M. Hosseini, "Laboratory studies of creep behavior on thick-walled hollow cylindrical salt rock specimens," *Arabian Journal of Geosciences*, vol. 8, pp. 1–9, 2015.

[14] D. Grgic and D. Amitrano, "Creep of a porous rock and associated acoustic emission under different hydrous conditions," *Journal of Geophysical Research: Solid Earth*, vol. 114, no. B10, 2009.

[15] S. Nadimi, K. Shahriar, M. Sharifzadeh, and P. Moarefvand, "Triaxial creep tests and back analysis of time-dependent behavior of Siah Bisheh cavern by 3-dimensional distinct element method," *Tunnelling and Underground Space Technology*, vol. 26, no. 1, pp. 155–162, 2011.

[16] J. Herrmann, E. Rybacki, H. Sone, and G. Dresen, "Deformation experiments on Bowland and Posidonia Shale—part II: creep behavior at in situ pc–T conditions," *Rock Mechanics and Rock Engineering*, vol. 53, no. 2, pp. 755–779, 2020,.

[17] E. Rybacki, J. Herrmann, R. Wirth, and G. Dresen, "Creep of Posidonia Shale at elevated pressure and temperature," *Rock Mechanics and Rock Engineering*, vol. 50, no. 12, pp. 3121–3140, 2017.

[18] D. R. Bhat and N. Bhandary, "Residual-state creep behavior of typical clayey soils," *Natural Hazards*, vol. 69, no. 3, pp. 2161–2178, 2013.

[19] M. Bagheri, M. Rezania, and M. Mousavi Nezhad, "An experimental study of the initial volumetric strain rate effect on the creep behaviour of reconstituted clays," *IOP Conference Series: Earth and Environmental Science*, vol. 26, 2015.

[20] G. Fabre and F. Pellet, "Creep and time-dependent damage in argillaceous rocks," *International Journal of Rock Mechanics and Mining Sciences*, vol. 43, no. 6, pp. 950–960, 2006.

[21] N. Brantut, P. Baud, M. J. Heap, and P. Meredith, "Micromechanics of brittle creep in rocks," *Journal of Geophysical Research (Solid Earth)*, vol. 117, no. B8, 2012.

[22] N. E. Davis, A. K. Kronenberg, and J. Newman, "Plasticity and diffusion creep of dolomite," *Tectonophysics*, vol. 456, no. 3-4, pp. 127–146, 2008.

[23] M. Smit, E. Scherer, T. John, and A. Janssen, "Creep of garnet in eclogite: mechanisms and implications," *Earth and Planetary Science Letters*, vol. 311, no. 3-4, pp. 411–419, 2011.

[24] E. Rybacki and G. Dresen, "Dislocation and diffusion creep of synthetic anorthite aggregates," *Journal of Geophysical Research*, vol. 105, no. B11, pp. 26017–26036, 2000.

[25] M. J. Heap, P. Baud, P. Meredith, A. Bell, and I. Main, "Time-dependent brittle creep in Darley Dale sandstone," *Journal of Geophysical Research*, vol. 114, no. B7, 2009.

[26] E. Brückl and M. Parotidis, "Prediction of slope instabilities due to deep-seated gravitational creep," *Natural hazards and earth system sciences*, vol. 5, no. 2, pp. 155–172, 2005.

[27] J. H. P. Bresser, "On the mechanism of dislocation creep of calcite at high temperature: inferences from experimentally measured pressure sensitivity and strain rate sensitivity of flow stress," *Journal of Geophysical Research: Solid Earth*, vol. 107, no. B12, pp. ECV 4-1–ECV 4-16, 2002.

[28] J.-P. Gratier, R. Guiguet, F. Renard, L. Jenatton, and D. Bernard, "A pressure solution creep law for quartz from indentation experiments," *Journal of Geophysical Research: Solid Earth*, vol. 114, no. B3, 2009.

[29] Y. Wu, L. Cheng, J. Killough et al., "Integrated characterization of the fracture network in fractured shale gas reservoirs–

stochastic fracture modeling, simulation and assisted history matching," *Journal of Petroleum Science and Engineering*, vol. 205, p. 108886, 2021.

[30] J. Lou, F. Gao, J. Yang, Y. Ren, and L. Yang, "Characteristics of evolution of mining-induced stress field in the longwall panel: insights from physical modeling," *International Journal of Coal Science & Technology*, vol. 8, 2021.

[31] H. Wu, G. Zhao, and W. Liang, "Mechanical properties and fracture characteristics of pre-holed rocks subjected to uniaxial loading: a comparative analysis of five hole shapes," *Theoretical and Applied Fracture Mechanics*, vol. 105, p. 102433, 2020.